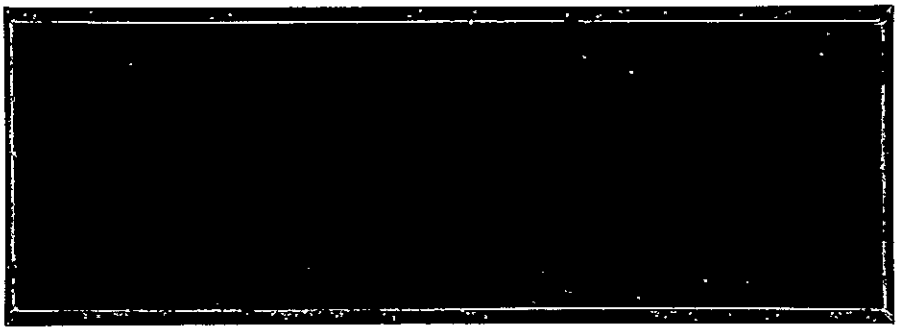

ELECTRICAL ENGINEERING

ENGINEERING EXPERIMENT STATION

AUBURN UNIVERSITY

AUBURN, ALABAMA

OPTICAL DATA PROCESSING STUDY

Contract No. : NAS8-31223
Control No. : 1-5-56-50731 (1F)
Inclusive Dates: 2-3-75 to 10-4-76

FINAL TECHNICAL REPORT

Author: L. J. Pinson

Submitted by: Department of Electrical Engineering
Auburn University
Engineering Experiment Station
Auburn, Alabama 36830

Date Submitted: October 12, 1976

Copy: _____ of _____

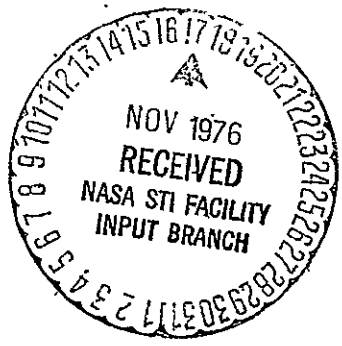

CONTENTS

1.0 INTRODUCTION

Satellite-borne, multi-spectral sensors such as found on the ERTS have produced a large volume of imagery which, if it is to be useful, must be transmitted to earth and analyzed. The large volume of this imagery has in fact created problems in how to best transmit, store and analyze the images. A useful alternative to this procedure is to perform on-board processing of the imagery for purposes of redundancy reduction or feature extraction. A successful on-board processing system would greatly reduce the load on transmission and storage systems.

The most promising candidate for on-board processing of images is a coherent optical data processing system. Such a system can effectively handle the large information content of imagery at high speeds. Evaluation and verification of coherent optical data processing for this application involves theoretical as well as experimental knowledge of the characteristics and limitations of the system. This program had the objective of establishing techniques and a knowledge base for performing this evaluation and verification of an optical data processing system designed to reduce redundancy in picture transmission and to detect specific image features.

Theoretically derived Fourier transform characteristics for simple but representative two-dimensional images serve as a basis for predicting expected features of actual target images. Typical targets to be considered might include linear patterns representative of rows of agricultural crops. Large area patterns of varying shapes could represent large scale terrain features. Targets of simple geometry were analyzed first. Further refinement such as inclusion of random dot patterns of varying sizes or certain

curvilinear patterns is, however, necessary for adequate modeling of actual imagery.

Fourier transformation and spatial filtering of coherent optical images is readily accomplished in theory and in the laboratory. The effect of various parameters such as optical aperture, incidence angles, the transparency assumption, and the thin lens approximation on resolution and performance of the optical data processing system were predicted and tested. An exhaustive parametric evaluation was not done, however, those parameters shown to be most critical to the system operation were evaluated thoroughly.

Thus, the program consisted of analytical and experimental evaluation of Fourier and correlation plane features in an optical data processing system for the purpose of redundancy reduction and pattern recognition. Figure 1 shows pictorially the main features of the program.

The following tasks were to be accomplished in fulfillment of the proposed optical data processing research effort.

Theoretical analysis

- Determine Fourier and correlation plane features to be expected from simple, but representative, target models.
- Determine expected parametric limitations as related to feature extraction in the Fourier and correlation planes.
- Study briefly detector geometry requirements as related to feature geometries.
- Investigate methods for combined analysis of Fourier and correlation plane information.

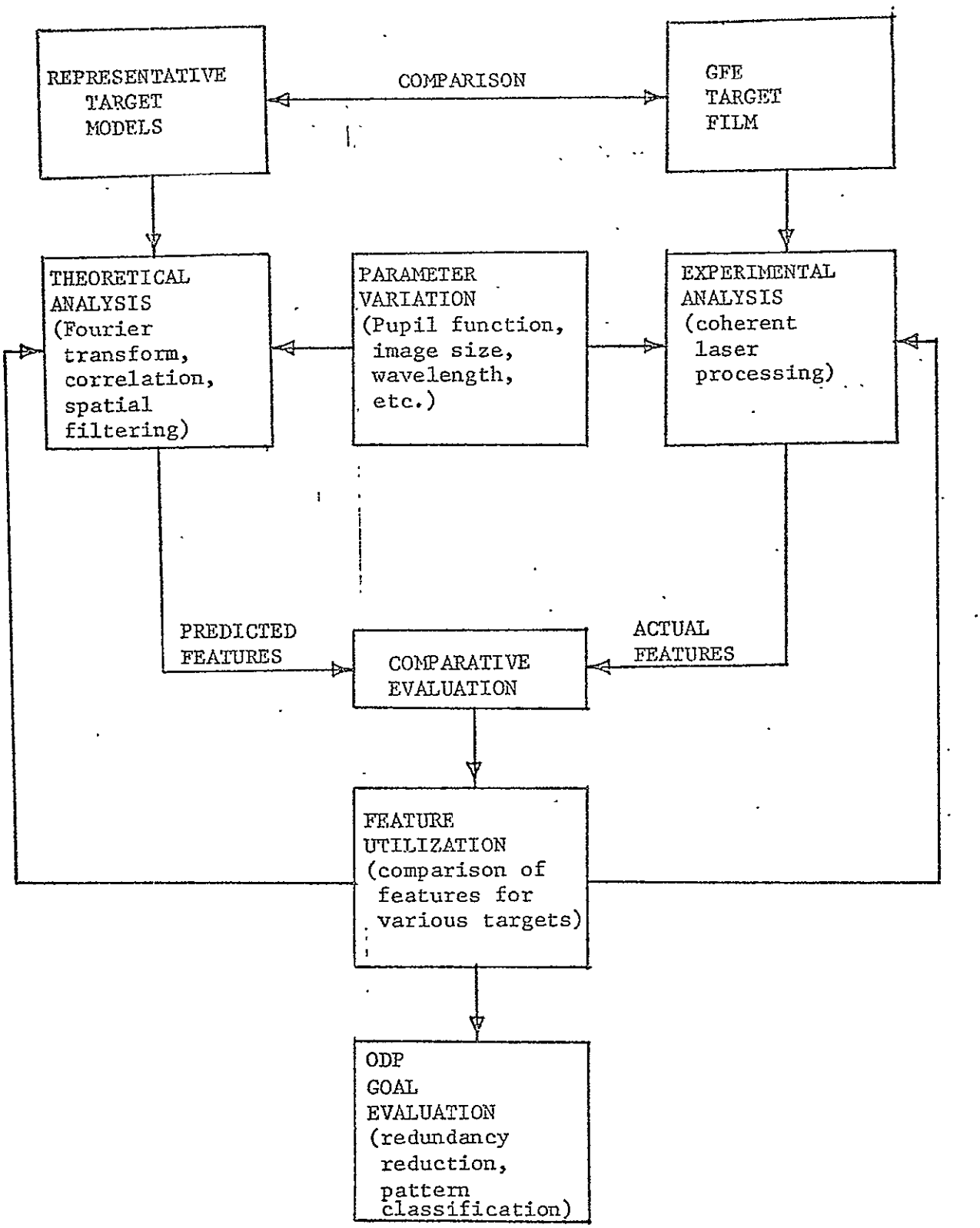

Figure 1: Flow Chart for Optical Data Processing Study

Experimental verification

- Using GFE target film, verify actual Fourier and correlation plane features for several target classifications.
- Compare experimental and theoretical features for representative targets.
- Implement and evaluate candidate methods for simultaneous analysis of Fourier and correlation plane features.

2:0 THEORETICAL ANALYSIS

The development of coherent light sources has made possible the processing of data using optical methods. That such processing methods as Fourier transformation, correlation, convolution and filtering can be achieved optically is not obvious and needs further justification. It is the purpose of this section to present a concise theoretical development showing that these processing methods can be implemented optically and to point out practical limitations to laboratory implementation of theoretically valid results.

No attempt is made to be complete in the description of the properties of coherent light. Rather the emphasis will be on techniques important to the goals of this contract. Additionally, the presentation is intended to be a concise reference useful to those persons familiar to some extent with coherent light systems and the mathematical development of Fourier transforms. All the information is available in scattered references, but nowhere is it available in as concise and readable (hopefully) a form as presented here.

Since light is a form of electromagnetic energy, a fundamental starting point for its description is Maxwell's equations. Through a series of assumptions (most of which can be imposed on a real system) and approximations the development leads to the Helmholtz equation and then the Fourier transforming properties of lenses. The assumptions and approximations are summarized in table form along with the result for easy reference.

Fourier transformation leads logically to correlation, convolution and filtering. Theoretical development of these operations is given.

The problems associated with the use of practical systems for data input, recording and filtering are discussed briefly along with parametric limitations.

Finally a brief theoretical introduction to advanced analysis methods which look at the fine structure of the optical correlation plane is given.

MAXWELL'S EQUATIONS, THE HELMHOLTZ EQUATION AND THE FOURIER TRANSFORMING PROPERTIES OF LENSES

Beginning with Maxwell's equations for a source free medium (Assumption #1)

$$\nabla \times \underset{\sim}{E} = \frac{-\partial \underset{\sim}{B}}{\partial t} \quad ; \quad \nabla \times \underset{\sim}{H} = \frac{\partial \underset{\sim}{D}}{\partial t} \tag{1}$$

It is convenient to use the temporal Fourier transforms of $\underset{\sim}{B}$ & $\underset{\sim}{D}$ to clear the time derivatives, i.e.

$$\nabla \times \hat{\underset{\sim}{E}}(\nu) = 2\pi i \nu \hat{\underset{\sim}{B}}(\nu) \quad ; \quad \nabla \times \hat{\underset{\sim}{H}}(\nu) = -2\pi i \nu \hat{\underset{\sim}{D}}(\nu) \tag{2}$$

where: $\left.\begin{matrix} \hat{\underset{\sim}{E}}(\nu) \text{ and } \underset{\sim}{E} \\ \hat{\underset{\sim}{B}}(\nu) \text{ and } \underset{\sim}{B} \end{matrix}\right\}$ are Fourier transform pairs.

Next we assume a non-dispersive (uniform) medium so the dependence on ν can be dropped. (Assumption #2)

Further if the medium is isotropic and linear we have (Assumption #3)

$$\hat{\underset{\sim}{D}} = \epsilon \hat{\underset{\sim}{E}} \quad \text{AND} \quad \hat{\underset{\sim}{B}} = \mu \hat{\underset{\sim}{H}} \tag{3}$$

Otherwise ϵ and μ are second rank tensors

From the differential equations in (2) we obtain the

VECTOR HELMHOLTZ EQUATIONS

$$\nabla^2 \hat{\underset{\sim}{E}} + 4\pi^2 k^2 \hat{\underset{\sim}{E}} = 0 \tag{4}$$

$$\nabla^2 \hat{\underset{\sim}{H}} + 4\pi^2 k^2 \hat{\underset{\sim}{H}} = 0 \tag{5}$$

For a three dimensional medium (such as an optical system) solution of the Vector Helmholtz Equations involves simultaneous solution of six scalar differential equations subject to a set of boundary conditions.

Solution of Vector Helmholtz Equations is impossible except for a few (impractical) cases; e.g., plane wave incident on perfect thin conducting half-plane.

Scalar Approximation - Assume the optical phenomenon of interest is adequately described by a scalar quantity. Note: the optical phenomenon of interest is normally the magnitude of the electric field vector expressed as a function of X, Y and Z coordinates and either time or frequency.

The scalar approximation results in the

SCALAR HELMHOLTZ EQUATION

$$\nabla^2 \hat{\phi} + 4\pi^2 k^2 \hat{\phi} = 0 \qquad (6)$$

where: $\hat{\phi} = \hat{\phi}(x,y,z,\nu)$

and $$\phi(x,y,z,t) = \int_{-\infty}^{\infty} d\nu \; e^{-2\pi i \nu t} \hat{\phi}(x,y,z,\nu) . \qquad (7)$$

ϕ is real; $\hat{\phi}$ is generally complex

If we assume a monochromatic field with temporal frequency $= \nu_o$, (Assumption #4)

then ϕ can be represented by

$$\phi(x,y,z,t) = \hat{\psi}(x,y,z)\, e^{-2\pi i \nu_o t} + \hat{\psi}^* e^{2\pi i \nu_o t}$$
$$= 2\, Re\left\{ \hat{\psi}(x,y,z)\, e^{-2\pi i \nu_o t} \right\} \qquad (8)$$

where: $\hat{\psi}(x,y,z)$ is a general complex spatial amplitude function.

For a plane wave, $\hat{\psi}(x,y,z)$ has the form

$$\hat{\psi}(x,y,z) = e^{2\pi i(\beta x + \gamma y + \eta z)}$$
$$= e^{2\pi i(\beta_x x + \beta_y y + \beta_z z)} \qquad (9)$$

then

$$\phi(x,y,z,t) = 2\,Re\left\{ e^{2\pi i(\beta_x x + \beta_y y + \beta_z z)} e^{-2\pi i \nu_0 t} \right\}$$
$$= 2\,Re\left\{ e^{2\pi i(\underset{\sim}{\beta}\cdot\underset{\sim}{r} - \nu_0 t)} \right\} \qquad (10)$$

The plane wave form of $\phi(x,y,z,t)$ satisfies the scalar Helmholtz equation if we impose the condition:

$$\underset{\sim}{\beta}\cdot\underset{\sim}{\beta} = k^2 = \frac{1}{\lambda^2} \quad ; \qquad (11)$$

k = wavenumber

λ = optical wavelength.

It can be shown that a sum of planewaves also satisfies the scalar Helmholtz equation, i.e.,

$$\hat{\psi}(x,y,z) = \sum_n A_n e^{2\pi i \underset{\sim}{k}_n \cdot \underset{\sim}{r}} \qquad (12)$$

where: $\underset{\sim}{k}_n = (\beta_{xn}, \beta_{yn}, \beta_{zn})$ wavenumber for nth planewave

$\underset{\sim}{r} = (x, y, z)$

and $\underset{\sim}{k}_n \cdot \underset{\sim}{k}_n = \frac{1}{\lambda^2}$ for all n

By taking this line of reasoning one step further, a continuous sum of planewaves also satisfies the scalar Helmholtz equation, i.e.,

$$\hat{\psi}(x,y,z) = \int d\underset{\sim}{k}\, A(\underset{\sim}{k})\, e^{2\pi i \underset{\sim}{k}\cdot\underset{\sim}{r}} \qquad (13)$$

Significance - Any optical function which can be represented as a sum of planewaves will satisfy the scalar Helmholtz equation.

Assumptions to this point (MEDIUM)	(OPTICAL FIELD)
1. source-free	1. adequately represented as a scalar quantity
2. isotropic	2. monochromatic
3. linear	3. can be represented as a summation of plane-waves
4. uniform (non-dispersive)	

Propagation of Optical Fields

Begin with the scalar Helmholtz equation given by equation (6)

$$\nabla^2 \hat{\phi} + 4\pi^2 k^2 \hat{\phi} = 0 \,. \tag{14}$$

Define $$\phi(x,y,z,t) = \hat{\psi}(x,y,z)\, e^{-2\pi i \nu_0 t} \,, \tag{15}$$

to separate temporal and spatial dependence (This form also implies a monochromatic field) with $\hat{\psi}(x,y,z)$ being the complex amplitude of the field.

Can verify that $\hat{\psi}(x,y,z)$ also satisfies the scalar Helmholtz equation, i.e.,

$$\nabla^2 \hat{\psi} + 4\pi^2 k^2 \hat{\psi} = 0 \tag{16}$$

Solve the boundary value problem for the field $\hat{\psi}(x,y,z)$ given $\hat{\psi}(x,y,0)$ as one of the boundary conditions. The result is the Rayleigh-Sommerfeld integral

$$\hat{\psi}(x,y,z) = -\frac{1}{2\pi} \int d\xi \int d\eta \; \hat{\psi}(\xi,\eta,0) \frac{\partial}{\partial z} \left\{ \frac{e^{2\pi i k s}}{s} \right\} \tag{17}$$

where : $$s = \left[(x-\xi)^2 + (y-\eta)^2 + z^2 \right]^{1/2}$$

Two approximations are now made to simplify (17) (See Figure 2)

Approximation 1: $(s/\lambda \gg 1)$ i.e., distance s is much greater than the optical wavelength.

Then we have the result known as Huygen's Principle

$$\hat{\psi}(x,y,z) \approx \frac{1}{i\lambda} \int d\xi \int d\eta \; \hat{\psi}(\xi,\eta,0) \cos(z,s) \frac{e^{2\pi i k s}}{s} \tag{18}$$

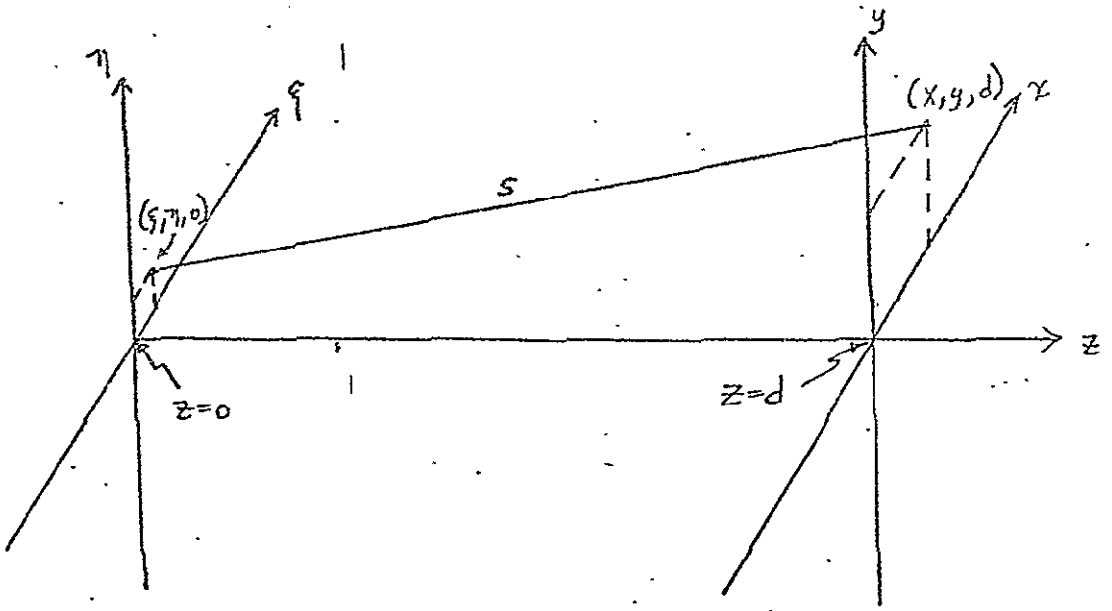

FIGURE 2 : PROPAGATION OF OPTICAL FIELDS

that is, the field at (X, Y, Z) is a weighted sum of spherical waves emanating from $(\xi, \eta, 0)$.

Approximation 2: (Fresnel approximation) at Z = d (Figure 2), assume the size of the regions of interest in either plane is small compared to d, i.e.,

$$\left[(x-\xi)^2 + (y-\eta)^2\right] << d^2 \tag{19}$$

then:

$$d \approx s$$
$$\cos(d,s) \approx 1$$
$$\frac{1}{s} \approx \frac{1}{d}$$

and the exponential term becomes approximately

$$s = d\left[1 + \frac{(x-\xi)^2+(y-\eta)^2}{d^2}\right]^{\frac{1}{2}}$$

$$\approx d + \frac{(x-\xi)^2+(y-\eta)^2}{2d} + [\text{higher order terms}]$$

Since $(x-\xi)$ & $(y-\eta)$ are small compared to d we can neglect the higher order terms and,

for exponent $$S \approx d + \frac{(x-\xi)^2 + (y-\eta)^2}{2d} \tag{20}$$

Substituting (20) into (18) gives

$$\hat{\psi}(x,y,z) \approx \frac{e^{2\pi i k d}}{i\lambda d} e^{\frac{i\pi(x^2+y^2)}{\lambda d}} * \hat{\psi}(x,y,0) \tag{21}$$

Equation (21) is the result of the Fresnel approximation and holds in the region close to the optical axis.

Recognize that (21) is (See Appendix A) $e^{2\pi i k d}$ times the Fresnel transform of $\hat{\psi}(x,y,0)$.

The constant phase term is usually ignored and the result is that <u>if the optical field is known in a given plane, it can be found in another plane by Fresnel transformation</u>.

<u>COMMENT</u>: The Fresnel approximation holds much better than expected. The reason is that for images with low spatial frequencies there is no longer a need to restrict the regions of interest to be close to the optical axis. <u>Most images of interest will fall in this category</u>.

<u>Fourier Properties of Lenses</u>

<u>Transparency Assumption</u> - Assume a thin lens has t(X, Y) transmission function consisting of the product of a pupil function and a pure phase term, i.e.,

$$\hat{t}(x,y) = \hat{p}(x,y)\, e^{i\phi(x,y)} \tag{22}$$

then the optical fields immediately before and after the lens are related by:

TRANSPARENCY ASSUMPTION

$$\hat{\Psi}_2(x,y,0_+) = \hat{t}(x,y)\,\hat{\Psi}_1(x,y,0_-) \tag{23}$$

THIN LENS APPROXIMATION

The thickness d(X, Y) of a lens with front and rear surface radii of curvature R_1 and R_2 is given by

$$d(x,y) = d_{MAX} + \left[R_2 - (R_2^2 - x^2 - y^2)^{\frac{1}{2}}\right] - \left[R_1 - (R_1^2 - x^2 - y^2)^{\frac{1}{2}}\right] \tag{24}$$

d_{max} is thickness at X = Y = 0

Approximate (24) for

$$x^2 + y^2 \ll R_2^2 \tag{25}$$

$$\& \quad x^2 + y^2 \ll R_1^2$$

by

$$d(x,y) \approx d_{MAX} - \frac{x^2+y^2}{2}\left(\frac{1}{R_1} - \frac{1}{R_2}\right) \tag{26}$$

Now the phase term in (22) is given by

$$\phi(x,y) = 2\pi k(n-1)\,d(x,y)$$

$$\approx 2\pi k(n-1)\,d_{MAX} - \pi k(x^2+y^2)(n-1)\left(\frac{1}{R_1} - \frac{1}{R_2}\right) \tag{27}$$

where: n = refractive index of lens material

k = wavenumber = $\frac{1}{\lambda}$

define: focal length

$$f \triangleq (n-1)\left(\frac{1}{R_1} - \frac{1}{R_2}\right) \tag{28}$$

then

$$\phi(x,y) \approx \frac{2\pi(n-1)d_{MAX}}{\lambda} - \frac{\pi(x^2+y^2)}{\lambda f} \tag{29}$$

If we combine the constant term in (29) into the pupil function given in (22) we have

$$\hat{t}(x,y) = \hat{p}(x,y)\, e^{-i\pi(x^2+y^2)/\lambda f} \qquad (30)$$

Equation (30) is the transmission function for a "thin" lens.

Now the focal plane response is found by

Incident field = $\hat{a}(\underset{\sim}{\chi})$ at front side of lens

After lens = $\hat{a}(\underset{\sim}{\chi})\,\hat{t}(\underset{\sim}{\chi})$

In focal plane

$$\hat{B}(\underset{\sim}{\chi}) = \frac{1}{i\lambda f}\, e^{i\pi\underset{\sim}{\chi}^2/\lambda f} * \hat{a}(\underset{\sim}{\chi})\,\hat{t}(\underset{\sim}{\chi}) \qquad (31)$$

Using $\hat{t}(\underset{\sim}{\chi})$ given in (30) and after cancellation of some terms the result is:

FOURIER TRANSFORM

$$\hat{B}(\underset{\sim}{\chi}) = \frac{e^{i\pi\underset{\sim}{\chi}^2/\lambda f}}{i\lambda f} \int d_{\underset{\sim}{\xi}}\, e^{-2\pi i\,\underset{\sim}{\xi}\cdot\underset{\sim}{\chi}/\lambda f}\, \hat{p}(\underset{\sim}{\xi})\,\hat{a}(\underset{\sim}{\xi}) \qquad (32)$$

This is the desired result. Except for the phase term outside the integral, equation (32) shows that the focal plane response is the Fourier transform of the product of the pupil function with the incident field, i.e.,

$$\boxed{\hat{B}\left(\frac{\underset{\sim}{\chi}}{\lambda f}\right) \overset{F.T.}{\Longleftrightarrow} \hat{p}(\underset{\sim}{\xi})\,\hat{a}(\underset{\sim}{\xi})} \qquad (33)$$

COMPLEX FILTERS, CONVOLUTION AND CORRELATION

COMPLEX FILTER GENERATION

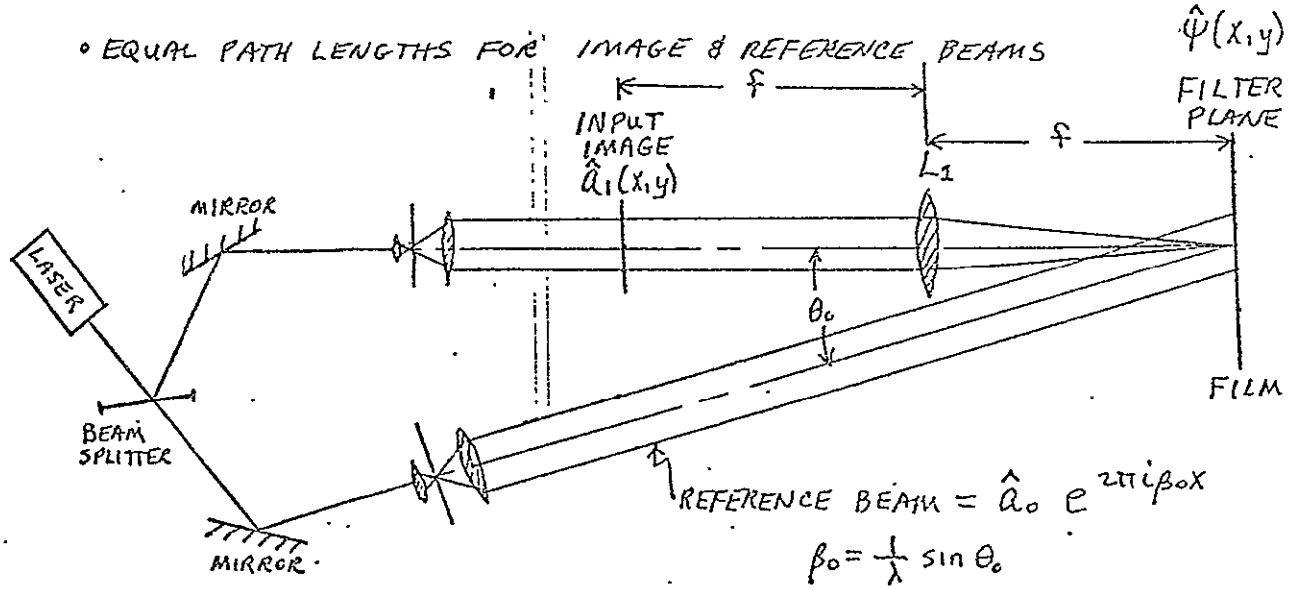

FIGURE 3 : COMPLEX FILTER GENERATION

Amplitude in the filter plane (See Figure 3) is the sum of the reference beam and the Fourier transform of $\hat{a}_1(x,y)$, i.e.,

$$\hat{\psi}(x,y) = \frac{1}{i\lambda f} \mathcal{F}\{\hat{a}_1(x,y)\} + \hat{a}_o e^{2\pi i \beta_o x} \qquad (34)$$

where: $\hat{a}_1(x,y)$ includes any pupil function;

or

$$\hat{\psi}(x,y) = \frac{1}{i\lambda f} \hat{A}_1\left(\frac{x}{\lambda f}, \frac{y}{\lambda f}\right) + \hat{a}_o e^{2\pi i \beta_o x} \qquad (35)$$

The photographic film in the filter plane is an energy sensitive medium thus the transmission of the developed negative is proportional to

$$\hat{T}(x,y) = 1 - |\hat{\Psi}(x,y)|^2$$
$$= 1 - \hat{\Psi}(x,y)\,\hat{\Psi}^*(x,y) \qquad (36)$$

Substituting in for $\hat{\Psi}$ we have

$$\hat{T}(x,y) = 1 - \left\{ \frac{1}{\lambda^2 f^2} \hat{A}_1\left(\frac{x}{\lambda f}, \frac{y}{\lambda f}\right) \hat{A}_1^*\left(\frac{x}{\lambda f}, \frac{y}{\lambda f}\right) + \hat{a}_o\,\hat{a}_o^* \right.$$
$$+ \frac{1}{i\lambda f} \hat{A}_1\left(\frac{x}{\lambda f}, \frac{y}{\lambda f}\right) \hat{a}_o^*\, e^{-2\pi i \beta_o x}$$
$$\left. - \frac{1}{i\lambda f} \hat{A}_1^*\left(\frac{x}{\lambda f}, \frac{y}{\lambda f}\right) \hat{a}_o\, e^{2\pi i \beta_o x} \right\} \qquad (37)$$

Through proper development of a positive transparency a transmission function proportional to $|\hat{\Psi}(x,y)|^2$ can be obtained. Either positive or negative transparencies will provide correlation results.

COMPLEX FILTERING

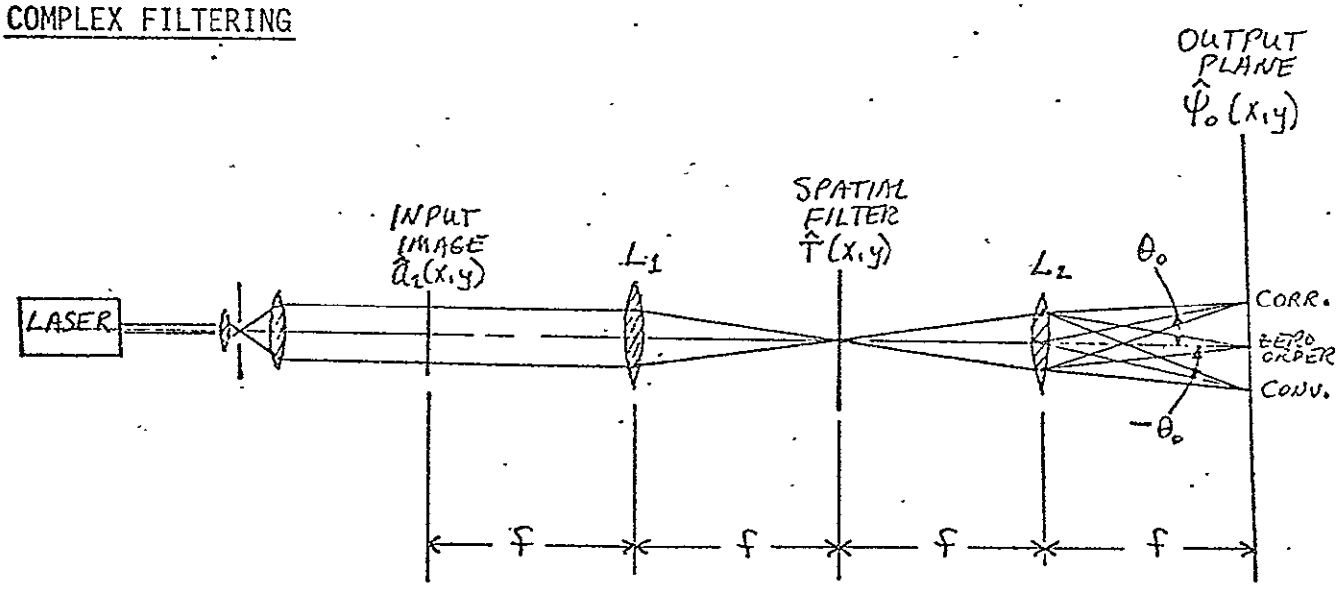

FIGURE 4: COMPLEX FILTERING

Figure 4 shows an arrangement for observing the cross correlation between images $\hat{a}_1(x,y)$ and $\hat{a}_2(x,y)$. It also gives the convolution of the two images.

The light amplitude immediately to the right of the spatial filter is given by:

$$\hat{A}_3\left(\frac{x}{\lambda f},\frac{y}{\lambda f}\right) = \hat{T}(x,y)\,\mathcal{F}\{\hat{a}_2(x,y)\} = \hat{T}(x,y)\,\frac{1}{i\lambda f}\,\hat{A}_2\left(\frac{x}{\lambda f},\frac{y}{\lambda f}\right)$$

$$= \frac{1}{i\lambda f}\left[1-\hat{a}_0\hat{a}_0^* - \frac{1}{\lambda^2 f^2}\hat{A}_1\left(\frac{x}{\lambda f},\frac{y}{\lambda f}\right)\hat{A}_1^*\left(\frac{x}{\lambda f},\frac{y}{\lambda f}\right)\right]\hat{A}_2\left(\frac{x}{\lambda f},\frac{y}{\lambda f}\right)$$

$$-\frac{1}{i\lambda f}\left[\frac{\hat{a}_0^*}{i\lambda f}\,\hat{A}_1\left(\frac{x}{\lambda f},\frac{y}{\lambda f}\right)e^{-2\pi i\beta_0 x}\right]\hat{A}_2\left(\frac{x}{\lambda f},\frac{y}{\lambda f}\right)$$

$$+\frac{1}{i\lambda f}\left[\frac{\hat{a}_0}{i\lambda f}\,\hat{A}_1^*\left(\frac{x}{\lambda f},\frac{y}{\lambda f}\right)e^{2\pi i\beta_0 x}\right]\hat{A}_2\left(\frac{x}{\lambda f},\frac{y}{\lambda f}\right) \qquad (38)$$

After transforming by lens L_2, equation (38) gives the following amplitude distribution in the output plane:

$$\hat{\psi}_0(x,y) = \frac{1}{i\lambda f}\int_{-\infty}^{\infty}\hat{A}_3(\beta,\gamma)\,e^{-2\pi i(\beta x+\gamma y)}\,d\beta\,d\gamma \qquad (39)$$

where:

$$\beta = \frac{x}{\lambda f}\quad,\quad \gamma = \frac{y}{\lambda f}\,.$$

THEN:

$$\hat{\psi}_0(x,y) = \left[\frac{(1-\hat{a}_0\hat{a}_0^*)}{i\lambda f}\,\hat{a}_2(x,y) - \frac{1}{i\lambda^3 f^3}\,\hat{a}_1(x,y)*\hat{a}_2(x,y)*\hat{a}_1(-x,-y)\right] \text{ ZERO ORDER TERMS}$$

$$+\left[\frac{\hat{a}_0^*}{\lambda^2 f^2}\,\hat{a}_1(x,y)*\delta(x+\beta_0\lambda f)*\hat{a}_2(x,y)\right] \text{ CONVOLUTION CENTERED @ } x=-\beta_0 f\lambda$$

$$-\left[\frac{\hat{a}_0}{\lambda^2 f^2}\,\hat{a}_1(-x,-y)*\delta(x-\beta_0\lambda f)*\hat{a}_2(x,y)\right] \text{ CROSS CORRELATION CENTERED @ } x=\beta_0 f\lambda \qquad (40)$$

Equation (40) is the desired result and for $\hat{a}_1(x,y) = \hat{a}_2(x,y)$ the resulting autocorrelation shows a strong peak at $X = \beta_0 f\lambda$. Because the spatial frequency content of most images is low, the resulting autocorrelation function appears simply as a bright spot. Energy detection for this so-called recognition spot is sufficient for distinguishing gross image differences. However, when comparing images that are quite similar, it is necessary to examine the fine structure of the correlation function to aid in distinguishing between these similar images. Examination of the fine structure of the correlation plane requires magnification, sampling and additional processing (probably by computer).

An alternate approach to the vander Lugt method for generation of optical correlation functions described above is discussed below.

Autocorrelation

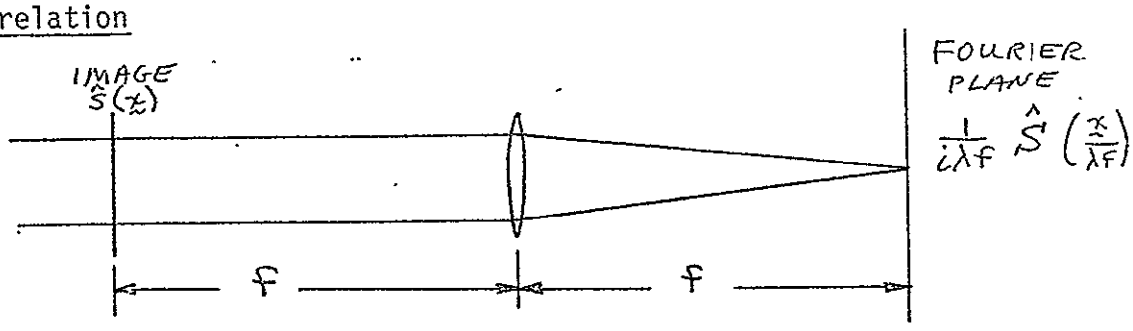

Figure 5: Power Spectrum Recording

The effect of the lens on the input image $\hat{s}(x)$ is to produce the Fourier transform $\frac{1}{i\lambda f}\hat{S}\left(\frac{x}{\lambda f}\right)$. Photographic film in the Fourier plane responds to intensity and after development has a transmittance proportional to

$$\hat{t}(\underset{\sim}{x}) \simeq \left| \frac{1}{i\lambda f} \hat{S}\left(\frac{\underset{\sim}{x}}{\lambda f}\right) \right|^2 = -\frac{1}{\lambda^2 f^2} \hat{S}\left(\frac{\underset{\sim}{x}}{\lambda f}\right) \hat{S}^*\left(\frac{\underset{\sim}{x}}{\lambda f}\right)$$

Or $\hat{t}(\underset{\sim}{x})$ is proportional to the power spectrum of the original image.

If this power spectrum transparency is viewed as shown in Figure 6

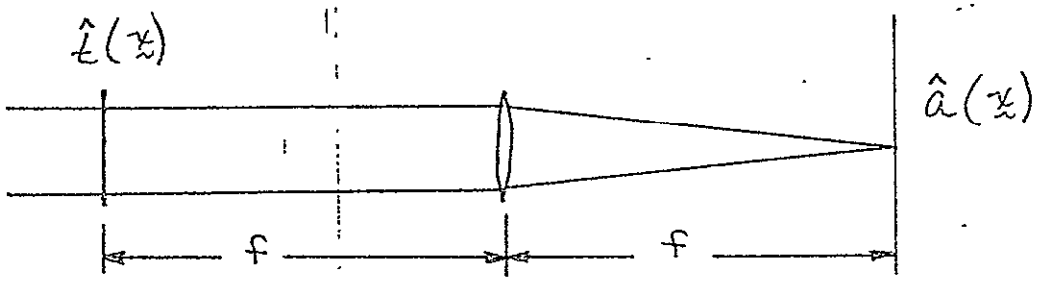

Figure 6: Autocorrelation

$$\hat{a}(\underset{\sim}{x}) = \frac{1}{i\lambda f} \mathcal{F}\{\hat{t}(\underset{\sim}{x})\} = -\frac{1}{i\lambda^3 f^3} \mathcal{F}\left\{\hat{S}\left(\frac{\underset{\sim}{x}}{\lambda f}\right) \hat{S}^*\left(\frac{\underset{\sim}{x}}{\lambda f}\right)\right\}$$

$$\boxed{\hat{a}(\underset{\sim}{x}) = -\frac{1}{i\lambda^3 f^3} R(\underset{\sim}{x})} \quad \text{AUTOCORRELATION}$$

Cross-Correlation

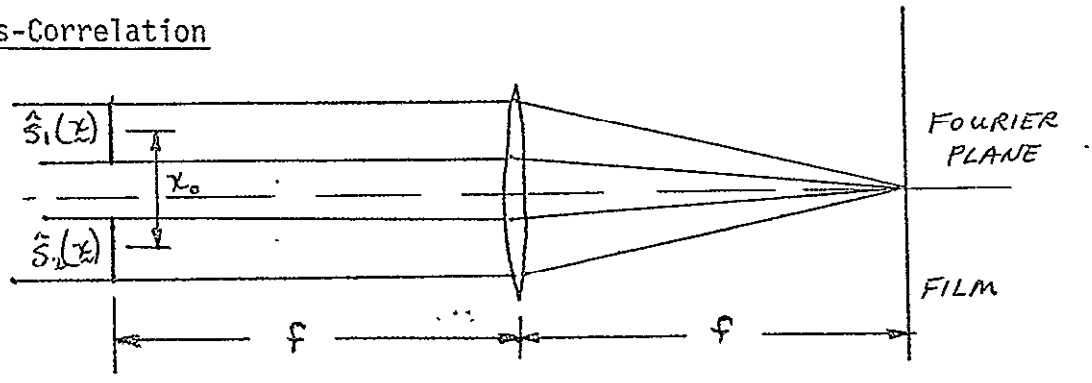

Figure 7: Generation of Cross Power Spectrum

Input

$$\hat{S}(x) = \hat{s}_1(x) * \delta\left(x - \frac{x_0}{2}\right) + \hat{s}_2(x) * \delta\left(x + \frac{x_0}{2}\right)$$

Field in Fourier plane

$$\frac{1}{i\lambda f}\hat{S}\left(\frac{x}{\lambda f}\right) = \frac{1}{i\lambda f}\left[\hat{S}_1\left(\frac{x}{\lambda f}\right)e^{-j\frac{2\pi x_0}{2\lambda f}} + \hat{S}_2\left(\frac{x}{\lambda f}\right)e^{j\frac{2\pi x_0}{2\lambda f}}\right]$$

Developed film transmittance

$$\hat{t}(x) \simeq \left|\frac{1}{i\lambda f}\hat{S}\left(\frac{x}{\lambda f}\right)\right|^2$$

$$\hat{t}(x) \simeq \frac{1}{\lambda^2 f^2}\left[\hat{S}_1\left(\frac{x}{\lambda f}\right)\hat{S}_1^*\left(\frac{x}{\lambda f}\right) + \hat{S}_2\left(\frac{x}{\lambda f}\right)\hat{S}_2^*\left(\frac{x}{\lambda f}\right) + \hat{S}_1\left(\frac{x}{\lambda f}\right)\hat{S}_2^*\left(\frac{x}{\lambda f}\right)e^{-j\frac{2\pi x_0}{\lambda f}} + \hat{S}_1^*\left(\frac{x}{\lambda f}\right)\hat{S}_2\left(\frac{x}{\lambda f}\right)e^{j\frac{2\pi x_0}{\lambda f}}\right]$$

Viewing

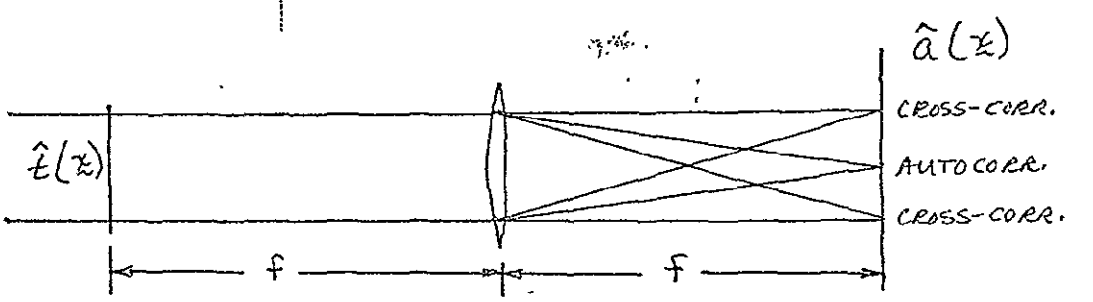

Figure 8. Cross Correlation

$$\hat{a}(x) = \frac{1}{i\lambda f}\mathcal{F}\{\hat{t}(x)\}$$

$$\hat{a}(x) = -\frac{1}{i\lambda^3 f^3}\left[R_1(x) + R_2(x) + R_{12}(x) * \delta(x - x_0) + R_{21}(x) * \delta(x + x_0)\right]$$

The relative strength of the cross correlation is strongly dependent on the degree of angular alignment in making the cross-spectrum transparency in Figure 7.

PRACTICAL CONSIDERATIONS

A number of parametric analyses can be derived from limitations imposed by practical systems and from approximations made in the theoretical development. Figures 9 through 14 are described below and provide parametric variations affecting the Fourier transforming properties of lenses. These figures were also included in Monthly Progress Report No. 5.

Figure 9. In order for no vignetting to occur certain restrictions must be placed on the input, output, and lens apertures. These relationships are depicted graphically where φ(max)/f is the (normalized) output aperture and r(max)/f is the (normalized) input aperture. Given a lens with a particular F-stop, r and φ must lie below that curve for no vignetting.

Fig. 9. Aperture restrictions for no vignetting

Figure 10 In the transform plane the spatial frequencies do not increase linearly with the distance from the optical axis. The per cent error in the linear frequency approximation is shown as a function of the output aperture size (normalized).

Figure 11 and Figure 12. These curves were derived using the exact expressions for the obliquity factor and the distance from the object point to the image point, (i.e., the Fresnel approximations were not made). Figure 11 shows the restrictions on input and output apertures (normalized) required to achieve a given maximum amplitude error in the transform plane. Figure 12 shows the phase term which multiplies the Fourier Transform expression for various values of focal length f.

Figure 13 Axial misalignment of the input plane from the lens results in a phase error in the transform plane, shown for various values d of maximum alignment error.

Figure 14 This figure shows the limits on frequency resolution for a perfectly aligned system. The limit is determined by the size of the aperture in the input plane.

The following parametric considerations apply to complex filtering.

Minimum reference beam angle - With reference to Figures 3 and 4 and equation (40), if both $\hat{a}_1(x,y)$ and $\hat{a}_2(x,y)$ have width, W, then separation of terms in the output plane of Figure 3 will be achieved if

$$\theta \geq \frac{5}{2}\frac{W}{f} \tag{41}$$

Fig. 10 - Accuracy of linear frequency approximation.

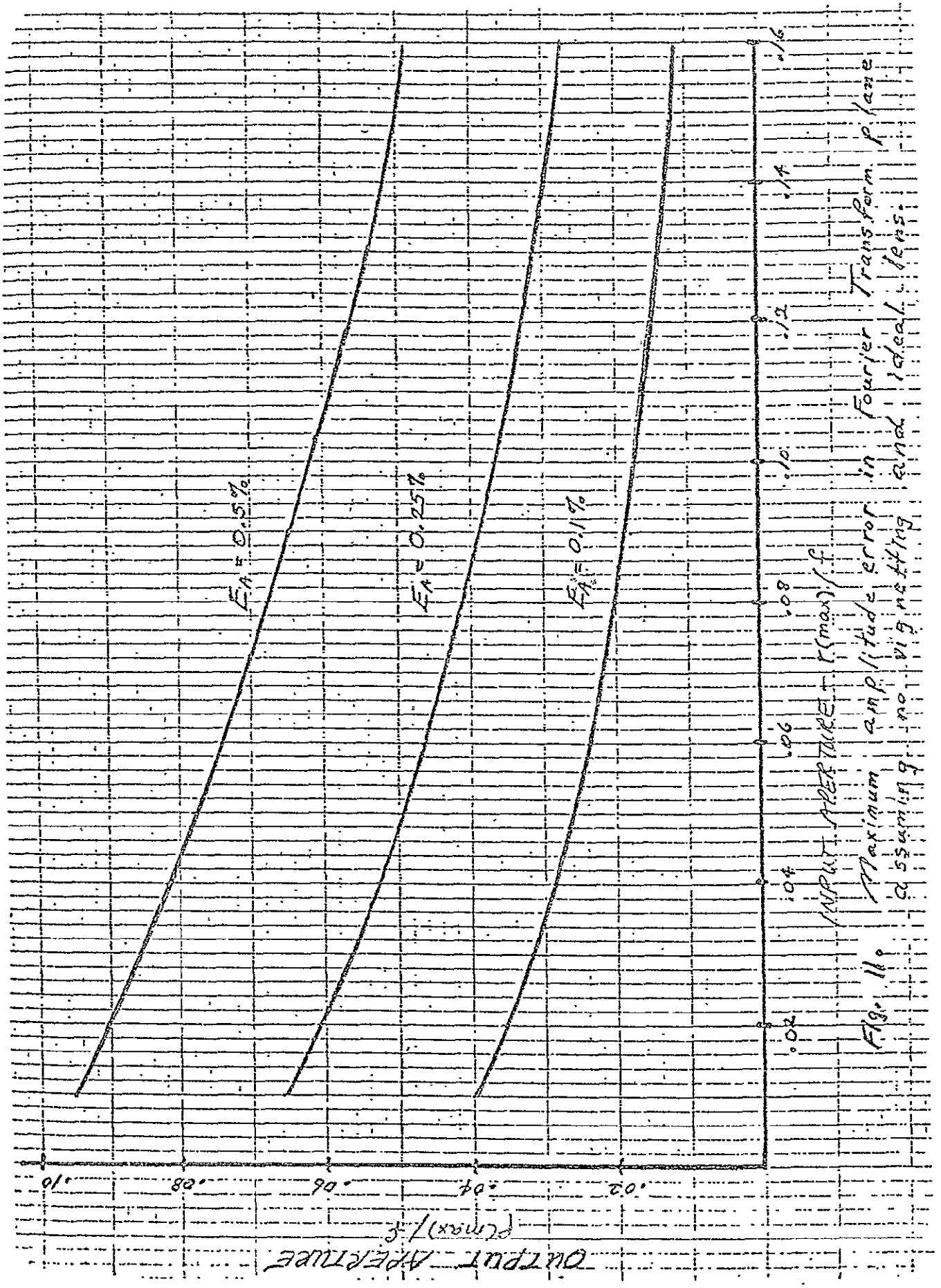

Fig. 11. Maximum amplitude error in Fourier Transform plane assuming no aliasing and equal lens apertures. INPUT APERTURE $r_{(max)}/f$

Fig. 12. Multiplicative phase term in Fourier Transform expression assuming ideal lens ($\lambda = 6328$ Å).

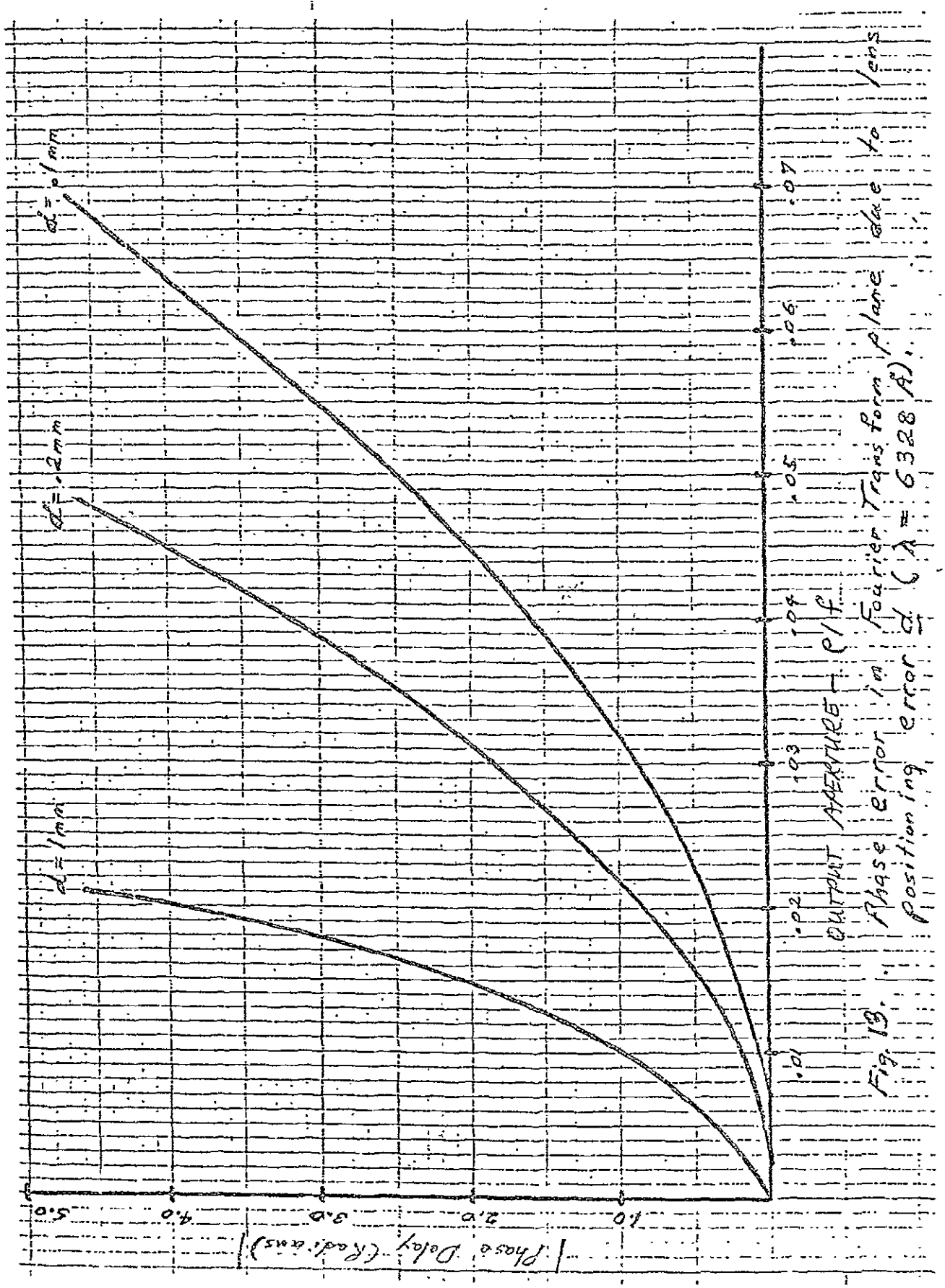

Fig. 13. Phase error in Fourier Transform plane due to positioning error of CM (λ = 6328 Å).

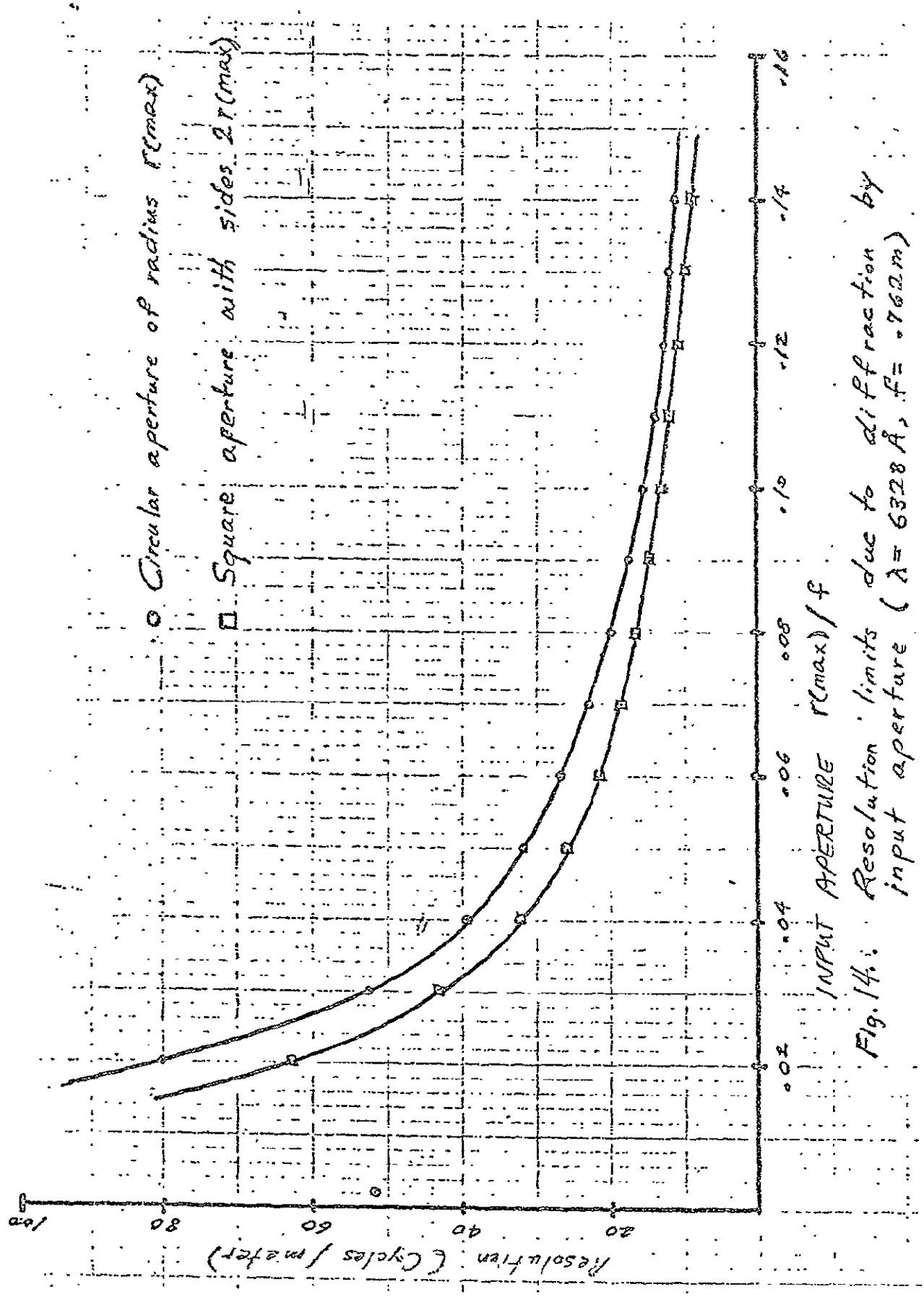

Fig. 14: Resolution limits due to diffraction by input aperture ($\lambda = 6328\,\text{Å}$, $f = .762\,m$)

Proof: In equation (40) we have

TWO ZERO-ORDER TERMS (centered at X, Y = 0, 0)

1st term has width W

2nd term has width 3W

CONVOLUTION TERM (centered at X, Y = $-\beta_o f\lambda$, 0)

has width 2 W

CORRELATION TERM (centered at X, Y = $\beta_o f\lambda$, 0)

has width 2W

Separation achieved if

$$\beta_o f\lambda - W \geq \frac{3}{2} W \tag{42}$$

or

$$\beta_o \lambda = \theta \geq \frac{5}{2} W \tag{43}$$

and finally with reference to Figure 4, a minimum aperture for lens L_2 can be established to ensure that the correlation and convolution terms of equation (40) fall within the lens aperture.

Film Resolution Requirements - For interference of two plane waves with angular separation α , the interference fringes are separated by

$$d = \frac{\lambda}{\sin \alpha} \tag{44}$$

Figure 15 shows a plot of the reciprocal of this equation for $\lambda = 6328\ \text{Å}$. It shows how resolution in cycles per millimeter increases as the reference angle α increases.

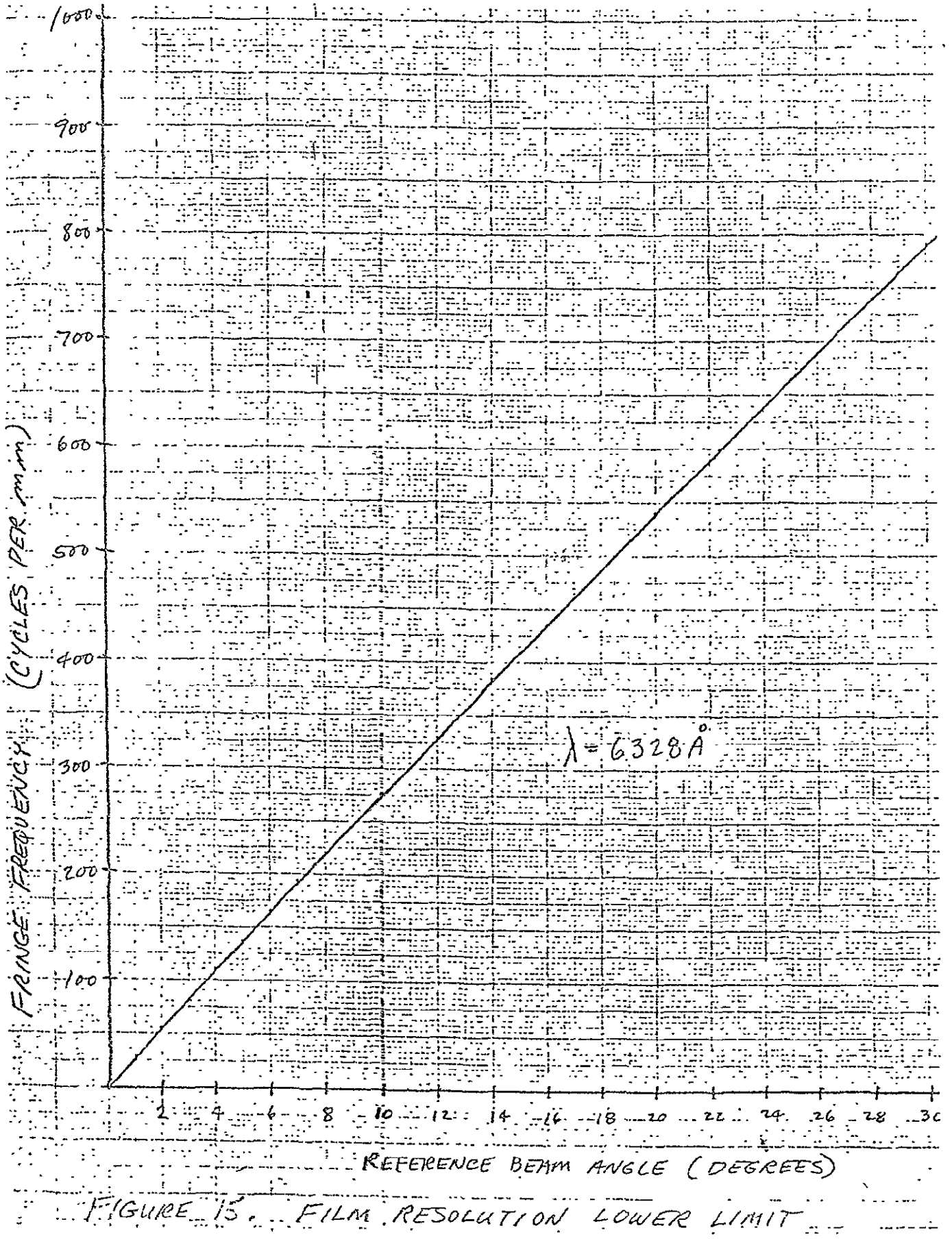

FIGURE 15. FILM RESOLUTION LOWER LIMIT

Effect of inherent phase term in Fourier transform expression - Even if the aperture restrictions are such that the amplitude error in the Fourier transform expression may be neglected and the linear frequency approximation is valid, there still exists a multiplicative phase term given by

$$e^{\left\{\frac{ikf}{4}\left(\frac{\varphi}{f}\right)^4\right\}} \tag{45}$$

which may not be neglected. However, the following development shows that this term is of no consequence in the operation of the optical correlator. [It does however affect the coherent imaging process.] Only the last term in the expression for $\hat{T}(x,y)$ will be considered since it is the term which will result in the correlation term in the output. To include the multiplicative phase factor this term should be written:

$$-\frac{1}{i\lambda f}\,\hat{A}_1^*\left(\frac{x}{\lambda f},\frac{y}{\lambda f}\right)\,\hat{a}_o\; e^{2\pi i\beta_o x}\; e^{-\frac{ikf}{4}\left(\frac{\varphi}{f}\right)^4} \tag{46}$$

When this is multiplied by the Fourier transform expression

$$\frac{1}{i\lambda f}\,\hat{A}_2\left(\frac{x}{\lambda f},\frac{y}{\lambda f}\right)\; e^{\frac{ikf}{4}\left(\frac{\varphi}{f}\right)^4} \tag{47}$$

these two additional phase terms cancel resulting in the original expression. Since a longitudinal positioning error of the input transparency results in a similar phase term, no error will result, providing the filter is recorded and all input signals are placed in the same longitudinally displaced position.

A similar statement may be made concerning lateral displacement of the input image. Since this lateral displacement results in the Fourier

transform expression being multiplied by a phase factor

$$e^{i2\pi\varphi d}$$

where d is the lateral displacement and φ is radial distance in the transform plane, then aslong as the recording and correlation processes take place using the same laterally displaced position, no error results. This is true because the phase term times its complex conjugate equals unity.

No analagous general statement can be made concerning angular positioning and rotation since these involve other than phase variations.

Two other types of displacements may occur in the input plane. These are angular displacements and rotations. Angular displacements result in the image plane no longer being perpendicular to the optical axis; whereas, rotations are defined to be angular movement about the optical axis which maintains perpendicularity. In general, the effects of these displacements are strongly dependent on the particular image function.

As an example, the periodic signal $\cos(2\pi\mu_x x)$ after being angularly displaced by the angle θ becomes the new signal

$$\cos\left(2\pi\mu_x \frac{x}{\cos\theta}\right) \tag{48}$$

In effect the "lines" of the signal have been "compressed" resulting in an expansion in the transform plane.

Effects of rotations in the input plane depend strongly on the signal since those signals with circular symmetry being correlated with themselves are immune to rotations while those with straight-line features may be affected greatly. Effects of rotation may be found for particular signals

$g(x,y)$ and $h(x,y)$ but little can be said in general since rotations may either increase or decrease the degree of correlation between two unlike signals. It might be noted that the effects of rotations (unlike lateral, longitudinal, and angular displacements) are the same (for a given rotation θ) whether the rotation takes place in the input or filter plane.

Filter displacements are much more critical than are image displacements between recording and correlation. In fact the above parametric effects of small image displacements assume that the filter is perfectly aligned. So critical is this alignment that it normally is accomplished with the aid of a microscope. The following development treats the effects of filter misalignments and is derived from A. Vander Lugt (Applied Optics, V.6, N.7, July 1967).

Figure 16. Shows relative correlation intensity for small lateral displacements of the filter for three ratios of image maximum size to focal length.

Figure 17. Shows relative correlation intensity for small longitudinal displacements of the optical filter as a function of image max. size to focal length ratio for three nominal displacements.

To determine the effect on performance of angular displacement of the filter, some previous results may be used. For a tilt of θ, the longitudinal displacement of the filter is given by

$$\Delta Z = \varphi(max) \tan\theta$$
$$\approx \varphi(max)\,\theta \qquad (49)$$

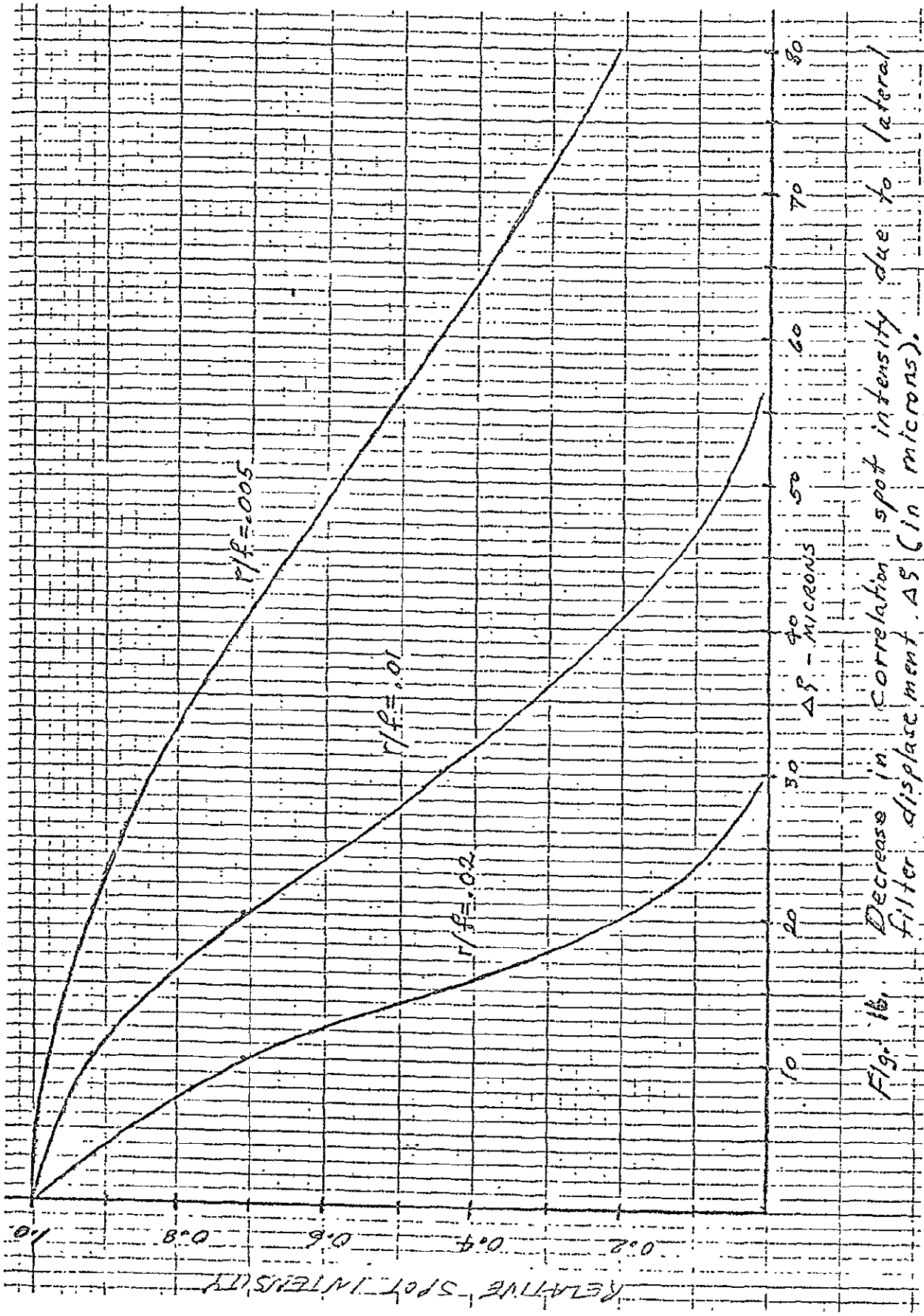

Fig. 16. Decrease in correlation spot intensity due to lateral filter displacement Δs (in microns).

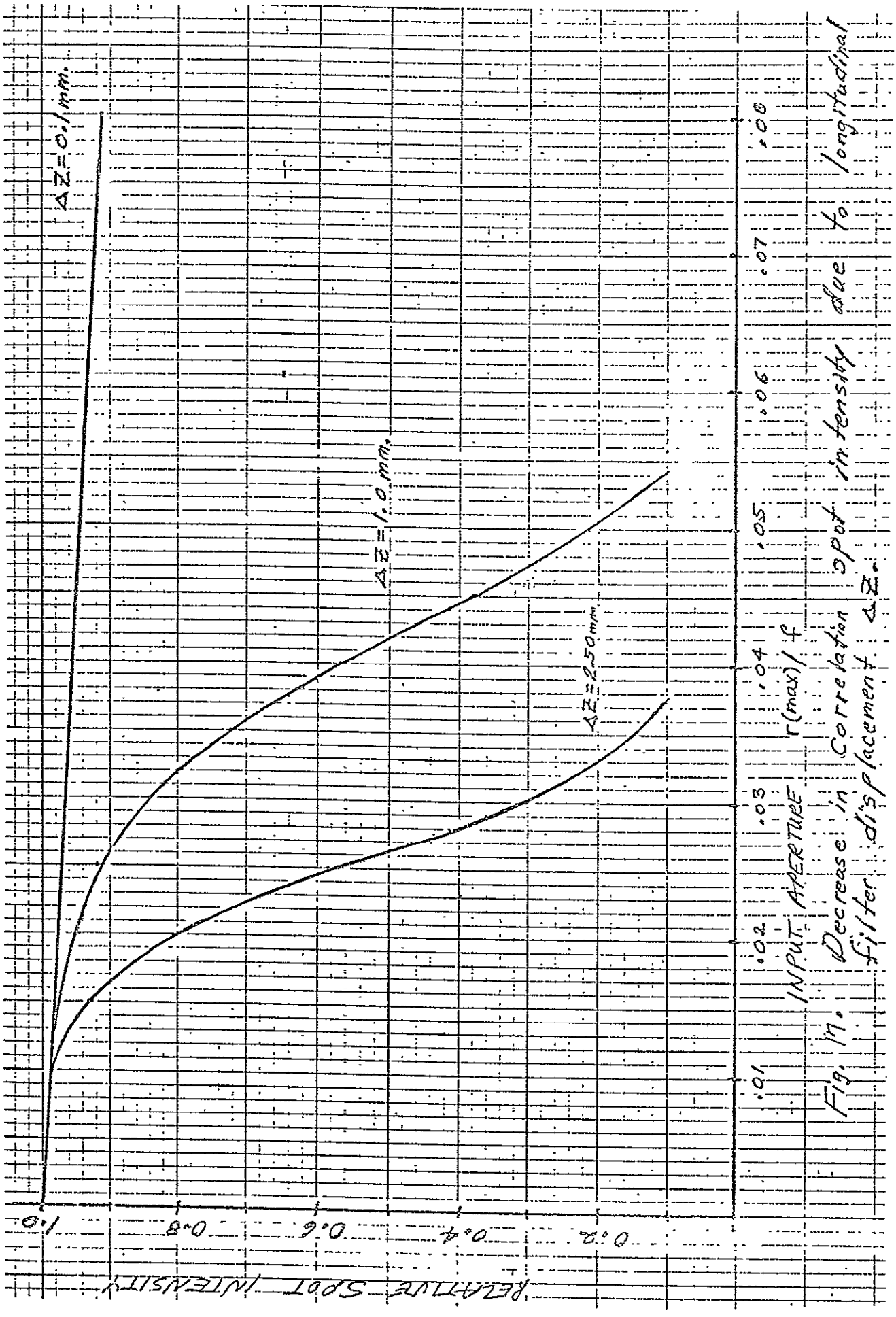

Fig. 17. Decrease in Correlation Spot Intensity due to Longitudinal Filter displacement ΔZ.

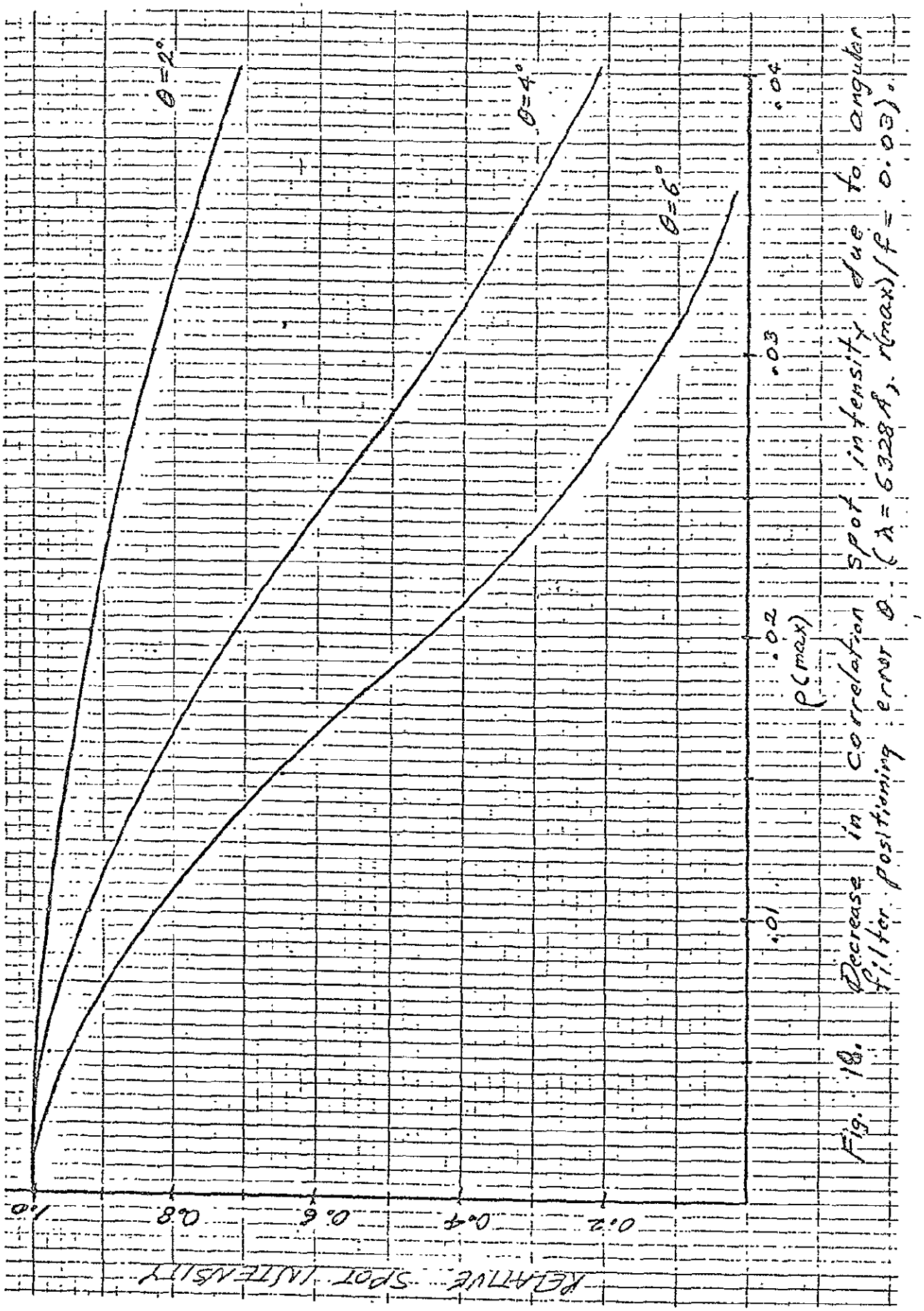

Fig. 18. Decrease in correlation of spot intensity due to angular tilt for positioning error θ. ($\lambda = 6328 \text{ Å}$, $r(\max)/f = 0.03$).

where $\varphi(\max)$ is the maximum extent of the Fourier Transform plane. Using this ΔZ in the longitudinal displacement equation yields performance for different θ (See Figure 18).

3.0 EXPERIMENTAL ANALYSIS

Experimental work on the program was impeded on several occasions because of construction and modification to the electro-optics laboratory. However, the major experimental tasks were accomplished. Improved results could have been obtained with more sophisticated auxiliary optical equipment such as precision positioning and alignment fixtures.

From the aerial photographs supplied by NASA, segments in 35 mm. format were selected which represent different types of terrain. For example, from the supplied photographs, several textures of cultivated land, orchards in various stages of development, forests, housing, motor vehicles and combined water-land areas were obtained. Since multiple shots of all photos were provided, the procedure was to simply cut example areas from one copy of each different photo. This method is simpler than a photographic reduction process and further has the advantage of retaining the resolution qualities of the larger format film. The only problem is that because of larger images the spatial frequency content will be more concentrated near the optical axis in the optical transform plane.

A total of eighteen representative segments were selected and optically transformed to check for significant differences and similarities among the various spectra. Photographs of the transforms were taken and enlarged/printed to facilitate comparison. Additionally, autocorrelation functions were generated optically and photographed for each of the candidate images. The method used for generating the correlation functions was to transform optically a photographic transparency of the power spectrum

for each image. This method eliminates alignment problems encountered in the Vander Lugt method for generating autocorrelation functions.

Cross-correlation functions may be generated in a similar fashion; however, there will be an alignment problem during recording of the cross-power spectrum.

A number of correlation experiments using the Vander Lugt method were conducted with the result being essentially the same for all experiments. That is, no recognition spot at all was obtained with any image except the one used to make the spatial filter. Even the auto-correlation spot was very weak in some cases, an effect most likely attributable to the previously mentioned alignment difficulties. The cross-correlation failed even for segments cut from the same larger image format (eg., two segments of a peach orchard). Enlarged photographs of selected aerial imagery, power spectra and autocorrelation functions are shown on the following pages. The need for more accurate alignment control is indicated by the results.

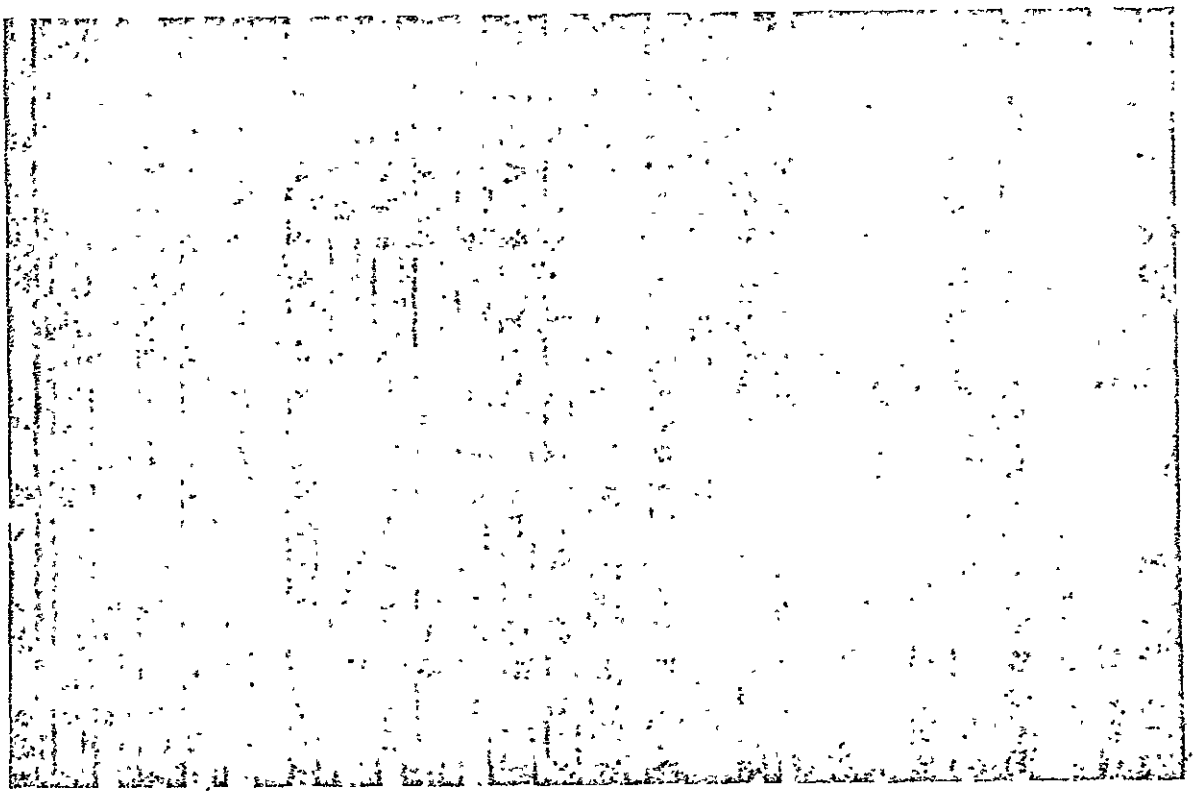

a.)

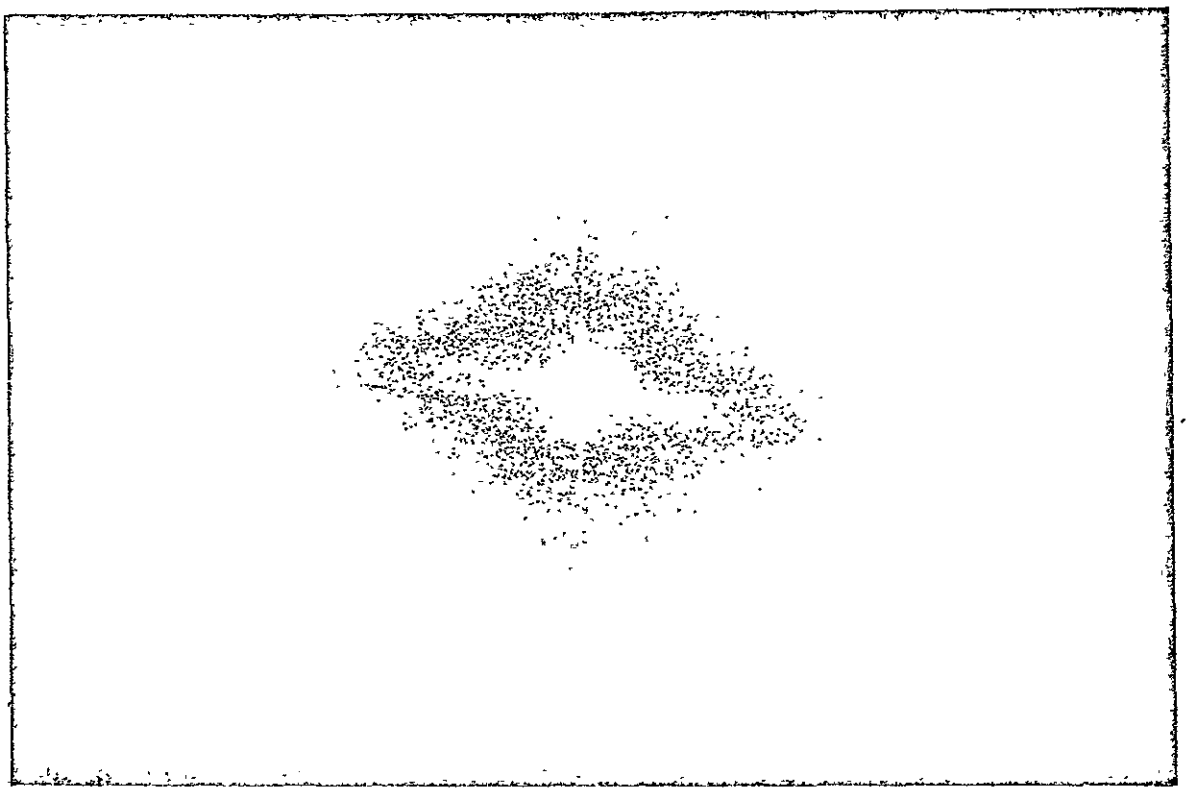

b.)

Figure 19. Peach Orchard (0132055, #3) a) image b) power spectrum c) autocorrelation

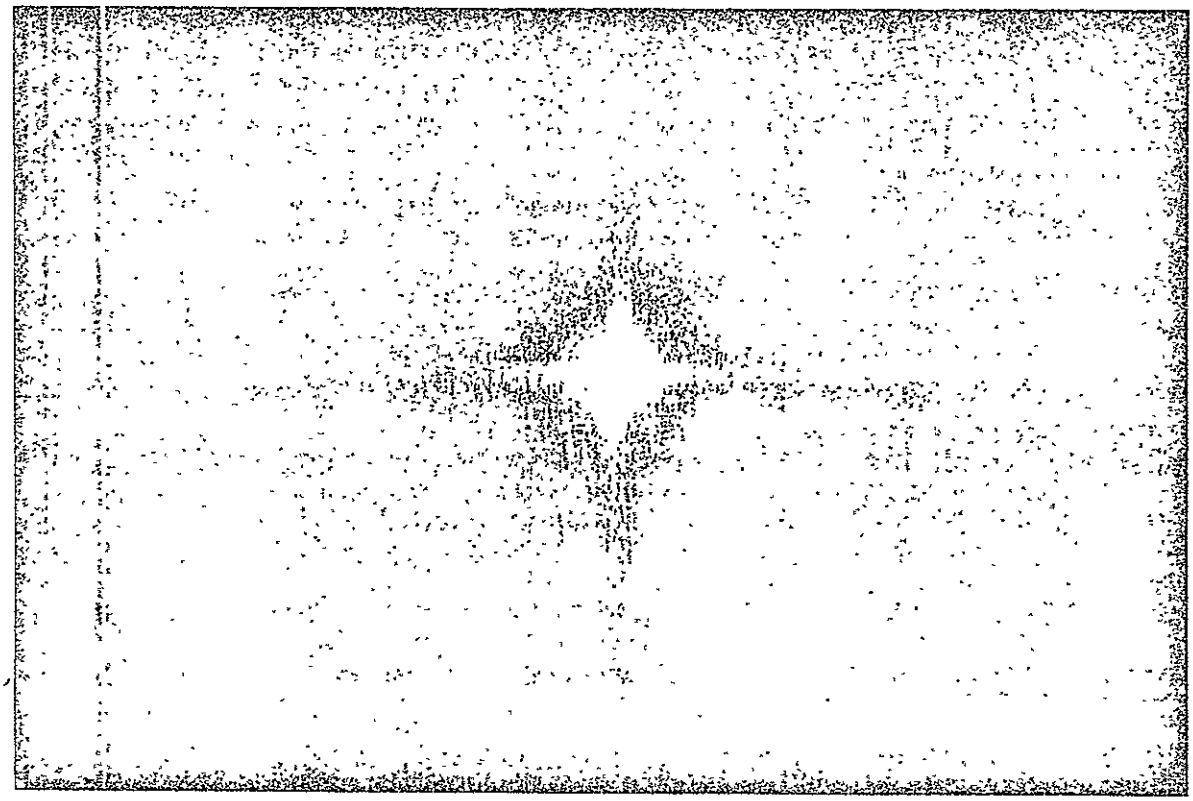

a.)

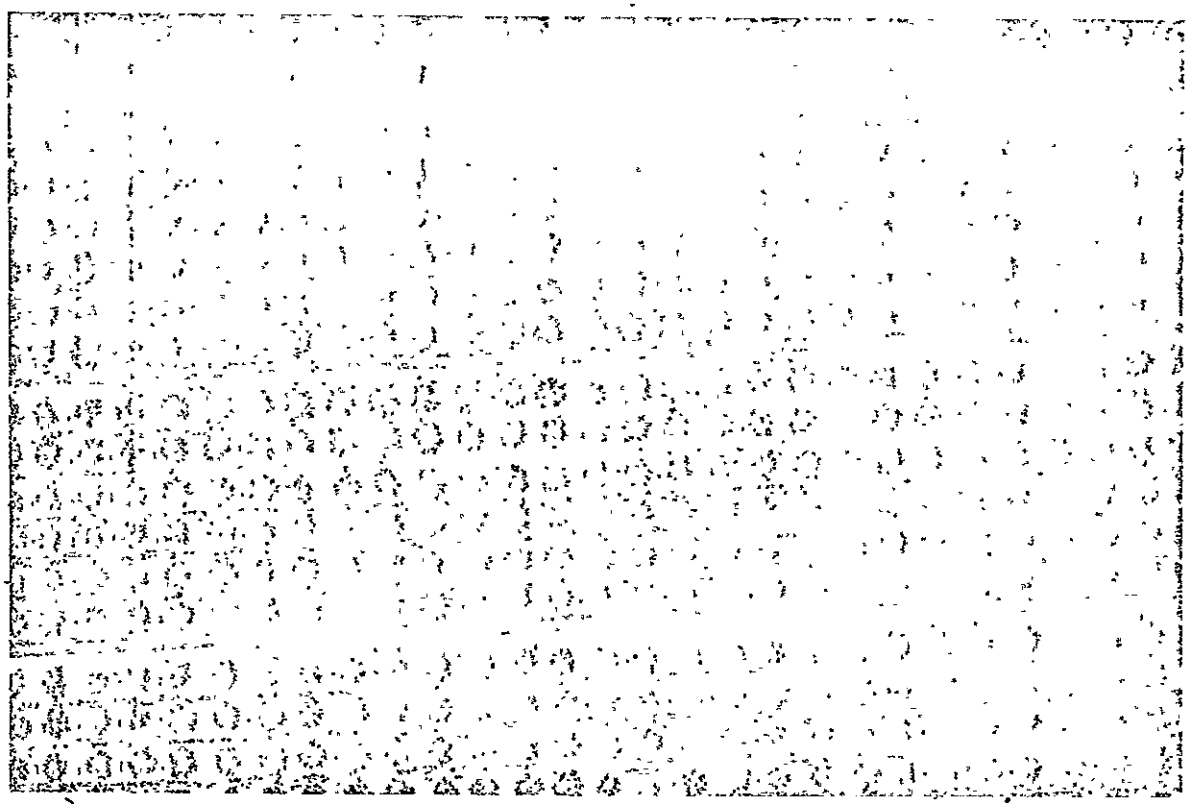

a.)

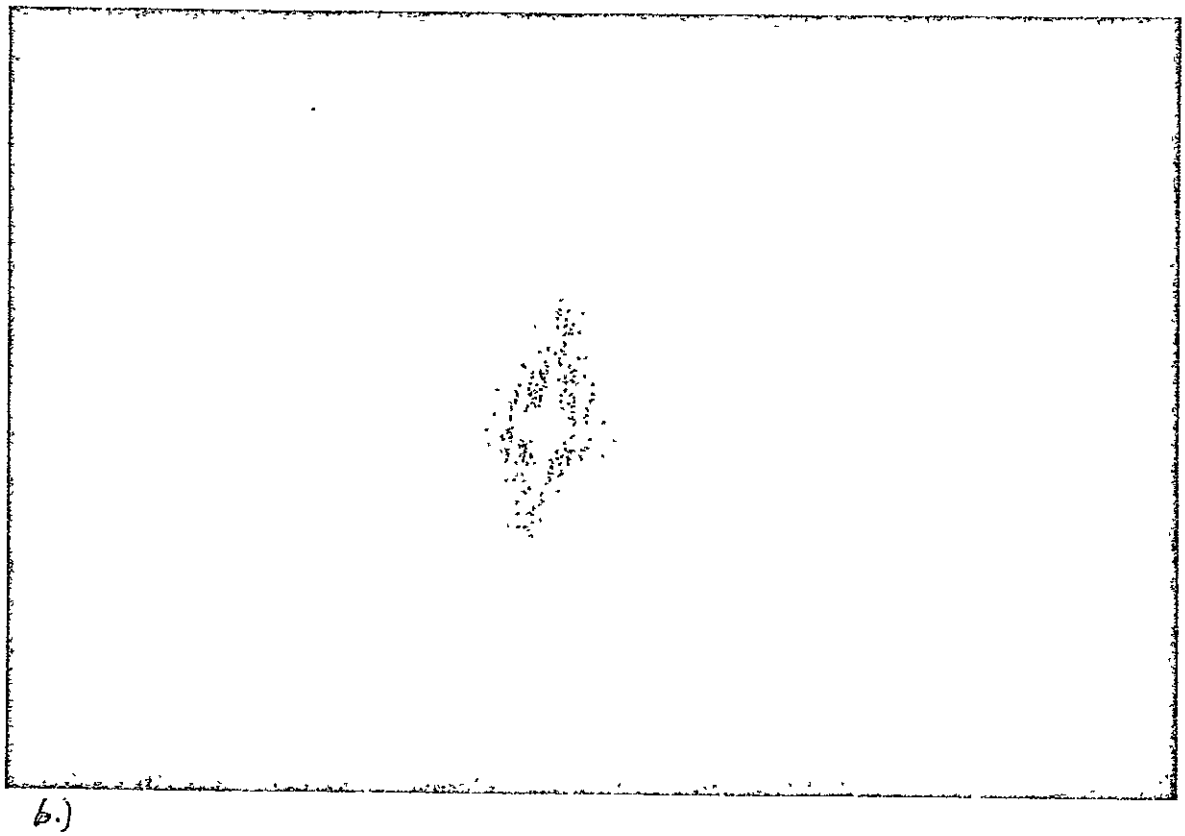

b.)

Figure 20. Peach Orchard (0132055, #1) a) image b) power spectrum c) autocorrelation

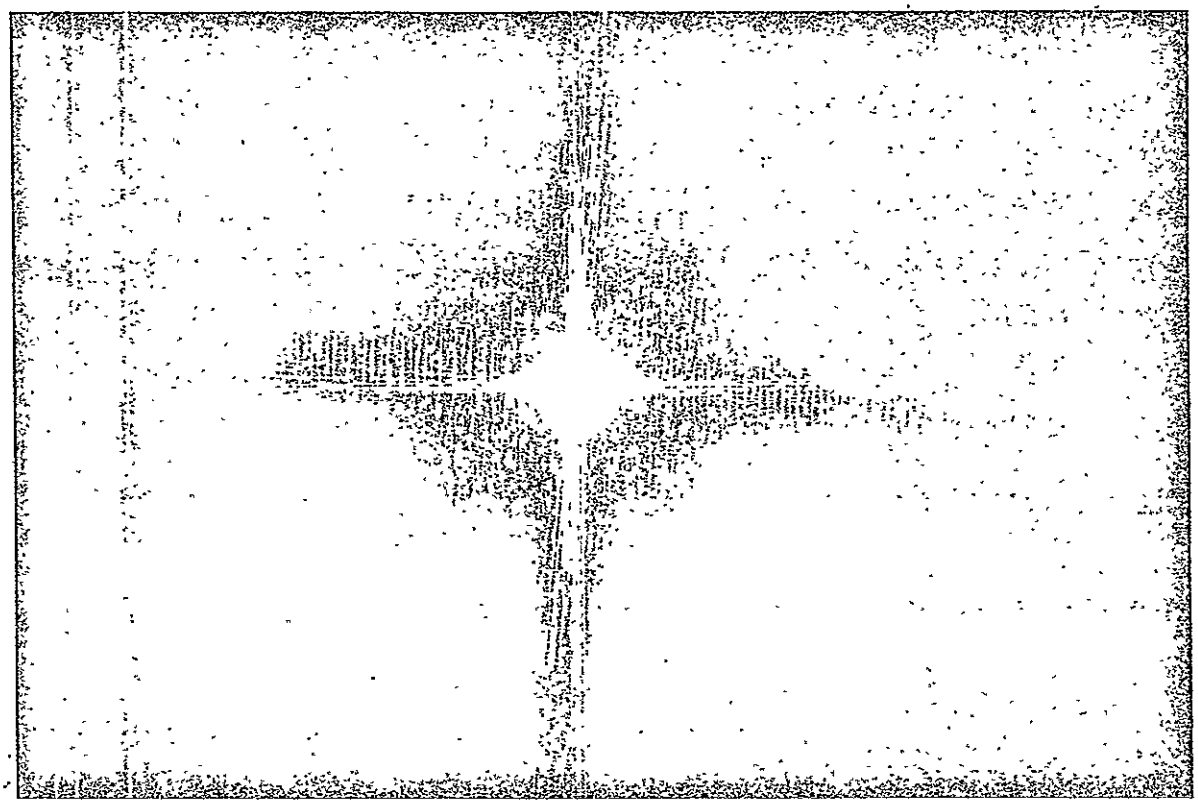

a)

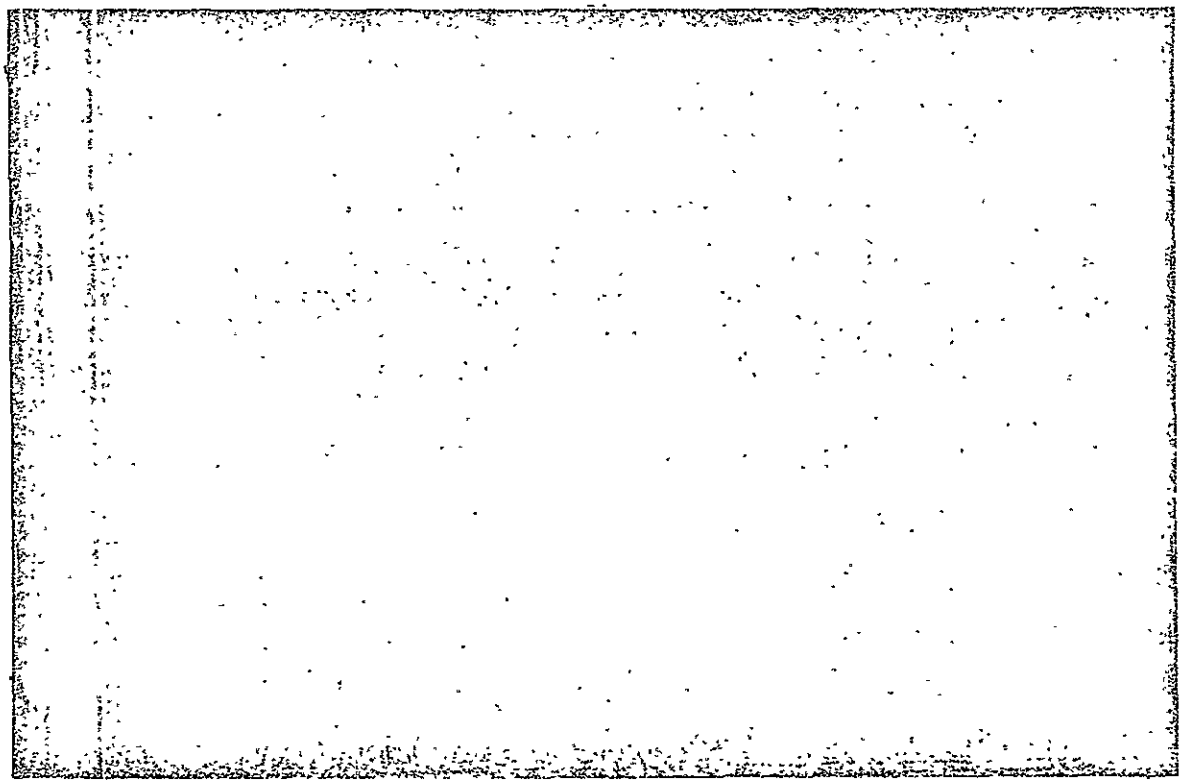

a.)

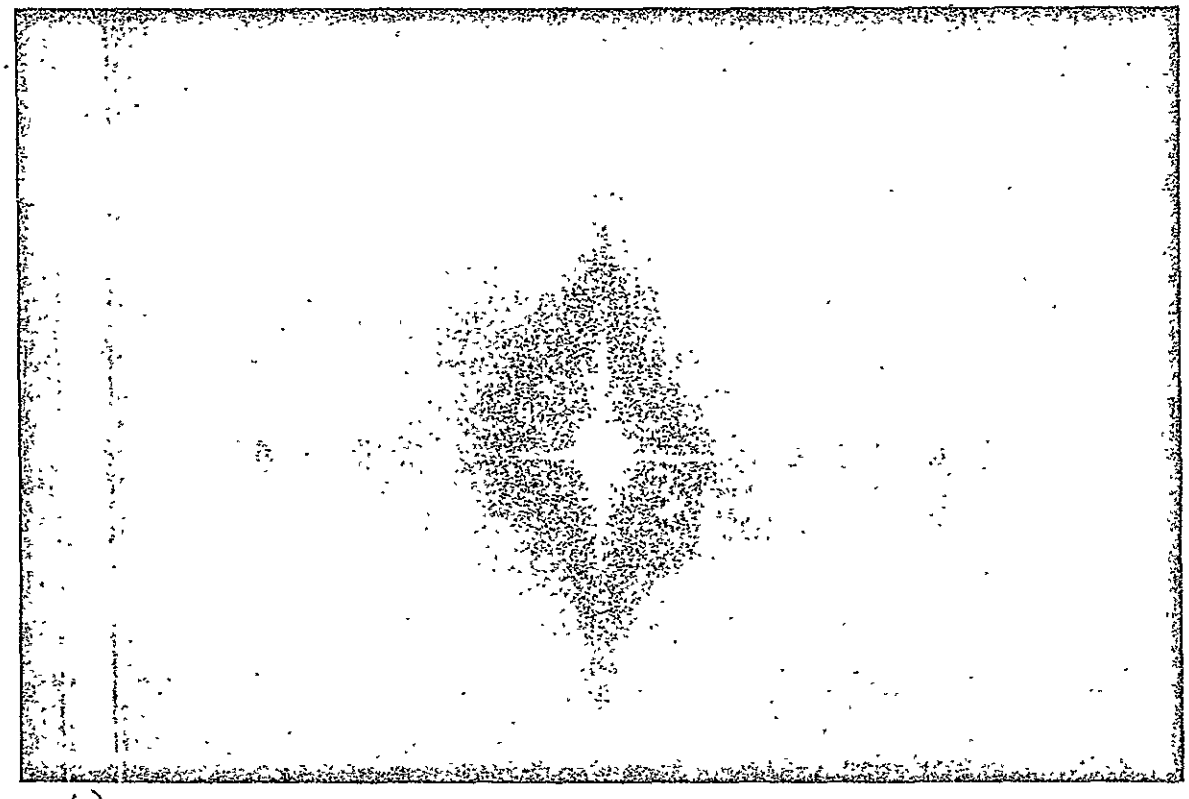

b.)

Figure 21. Plowed field (01320063, #1) a) image b) power spectrum c) autocorrelation

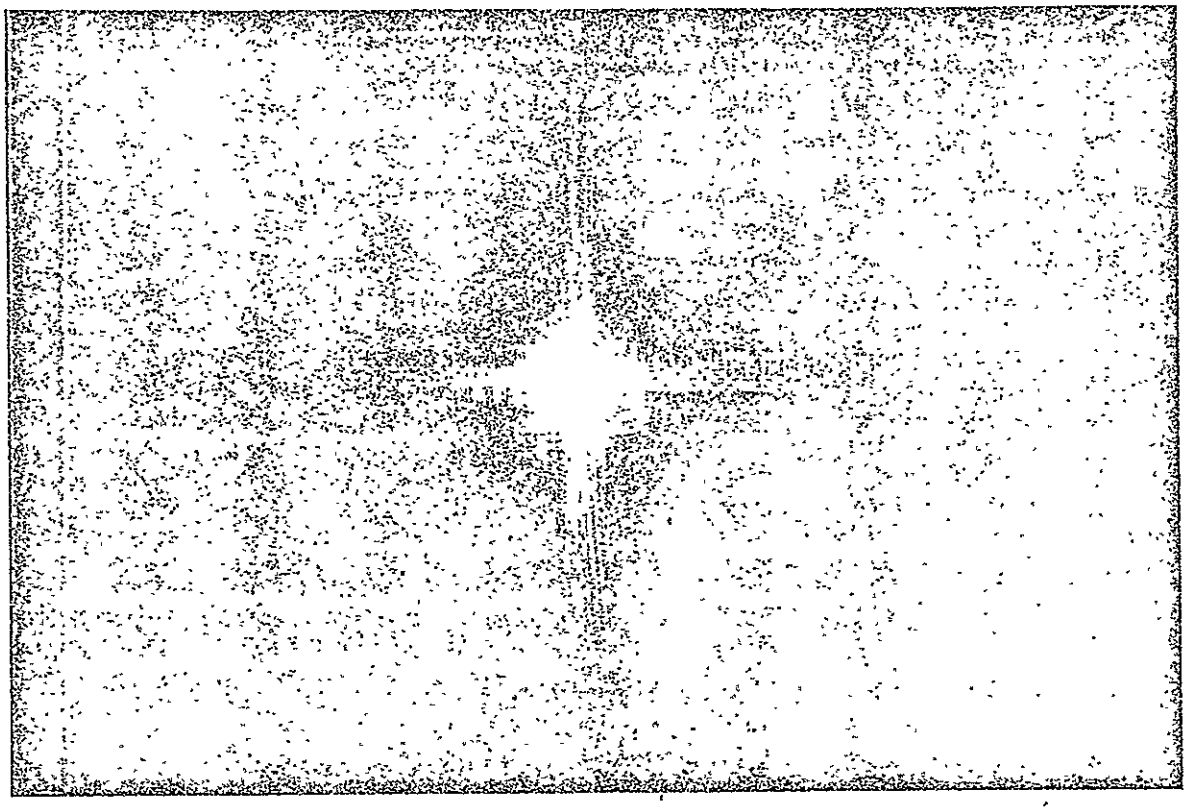

a)

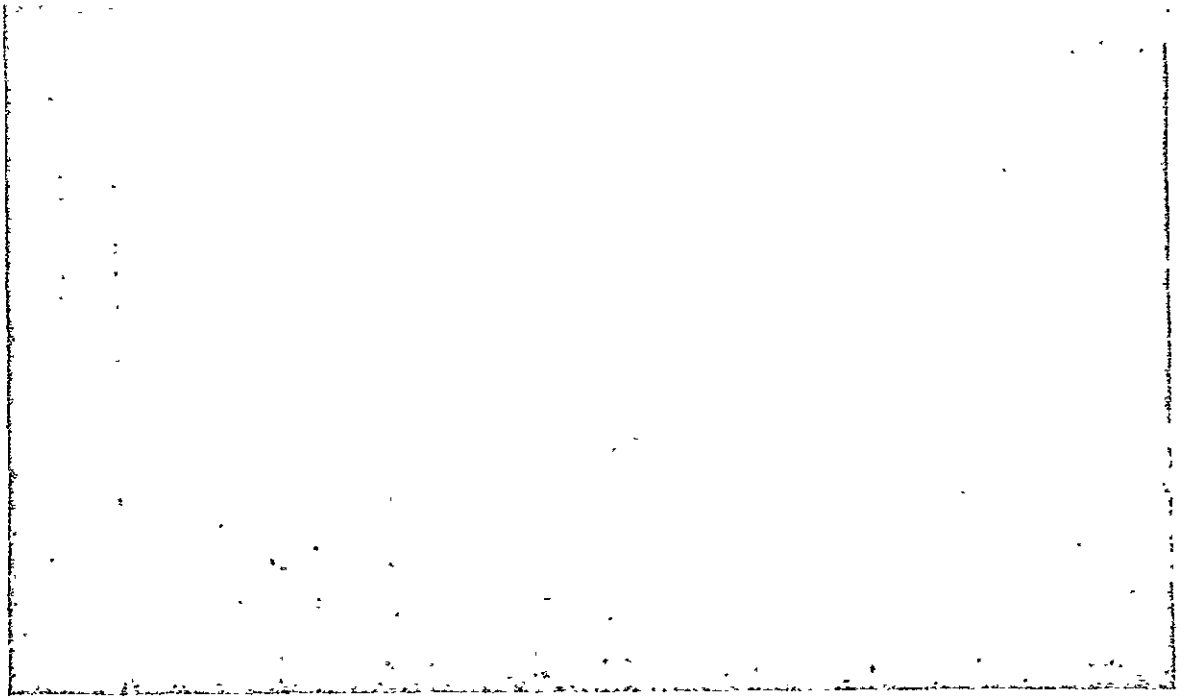

a.)

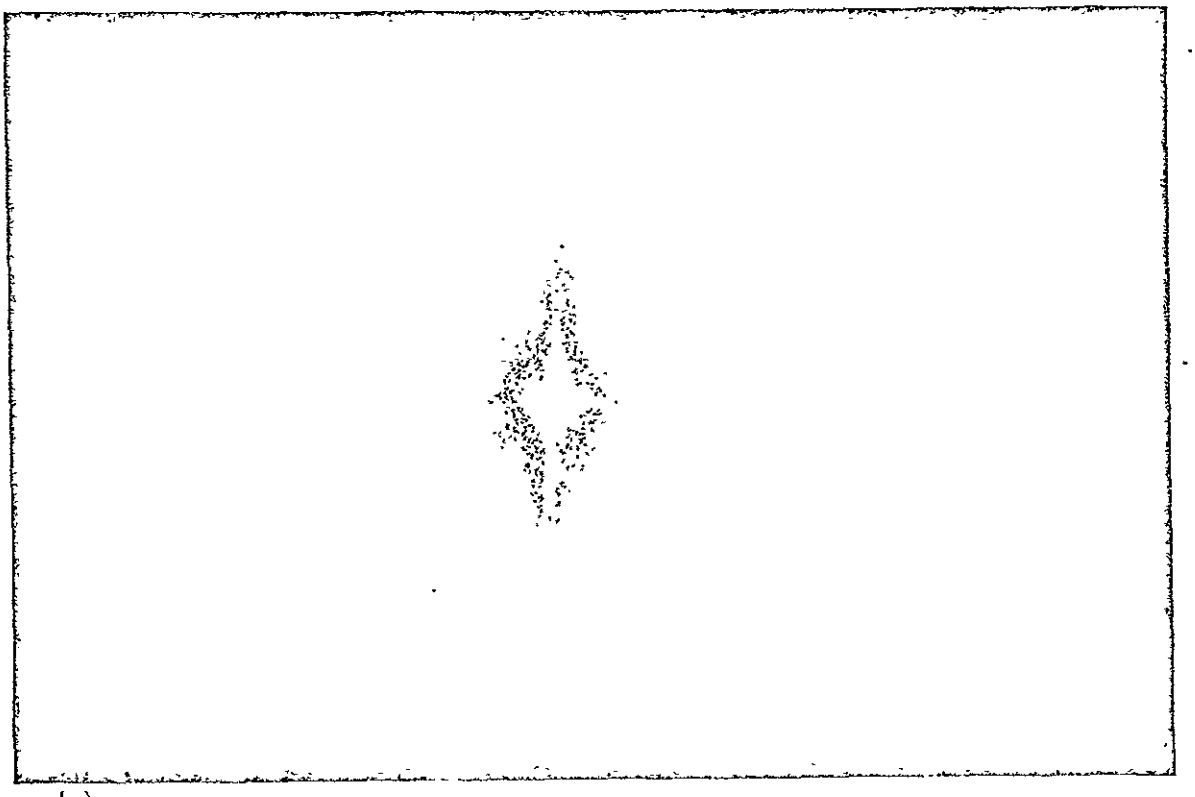

b.)

Figure 22. Pasture (01320063, #3) a) image b) power spectrum c) autocorrelation

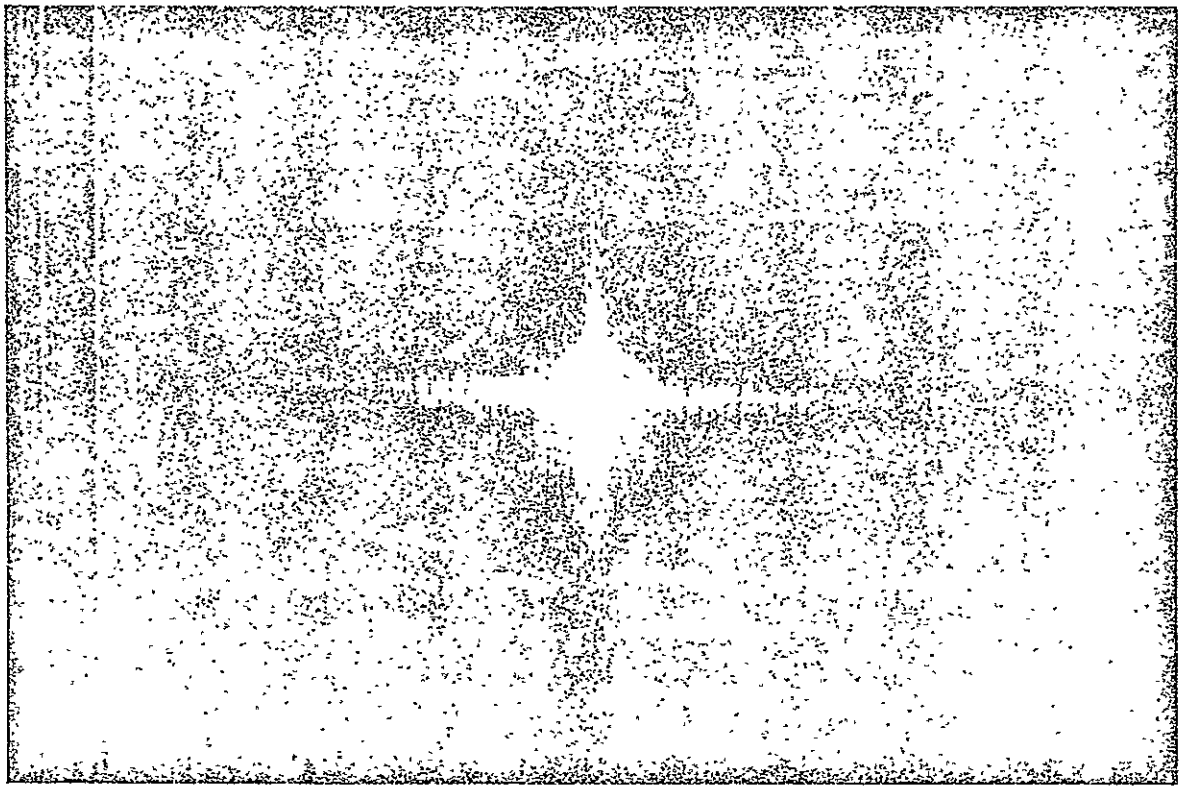

a.)

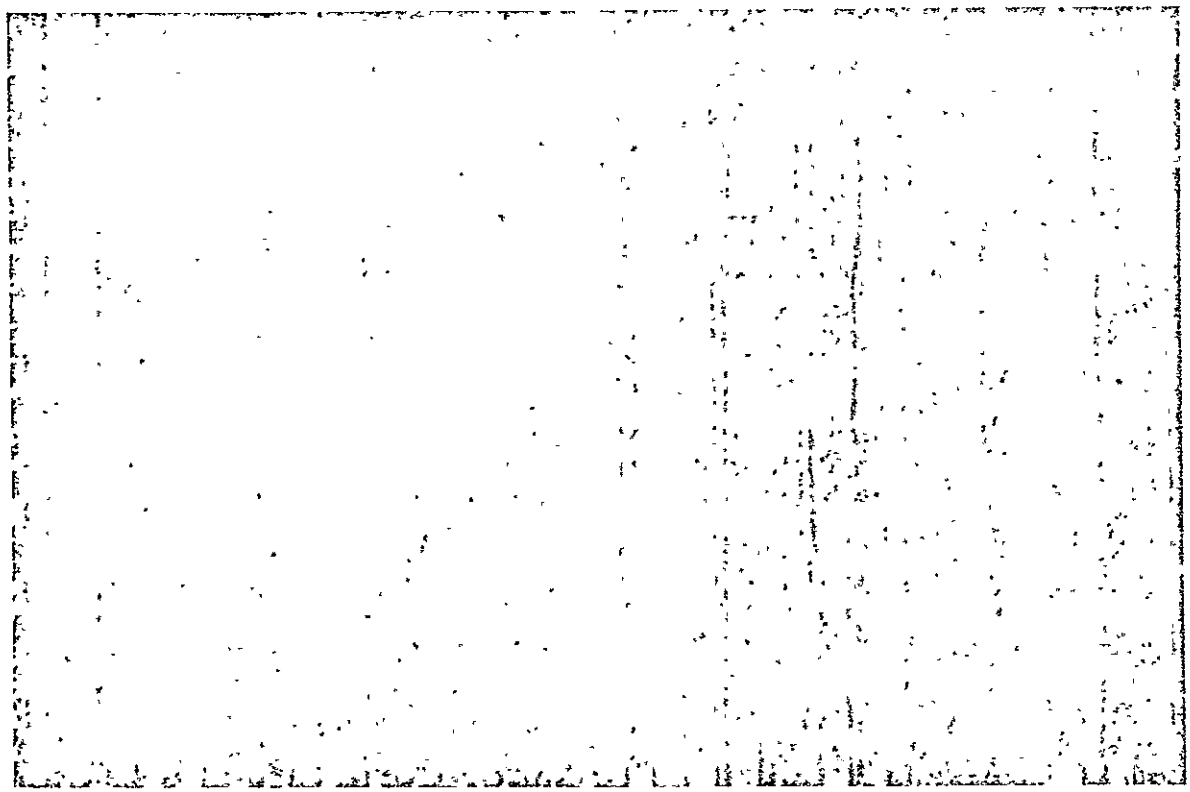

a.)

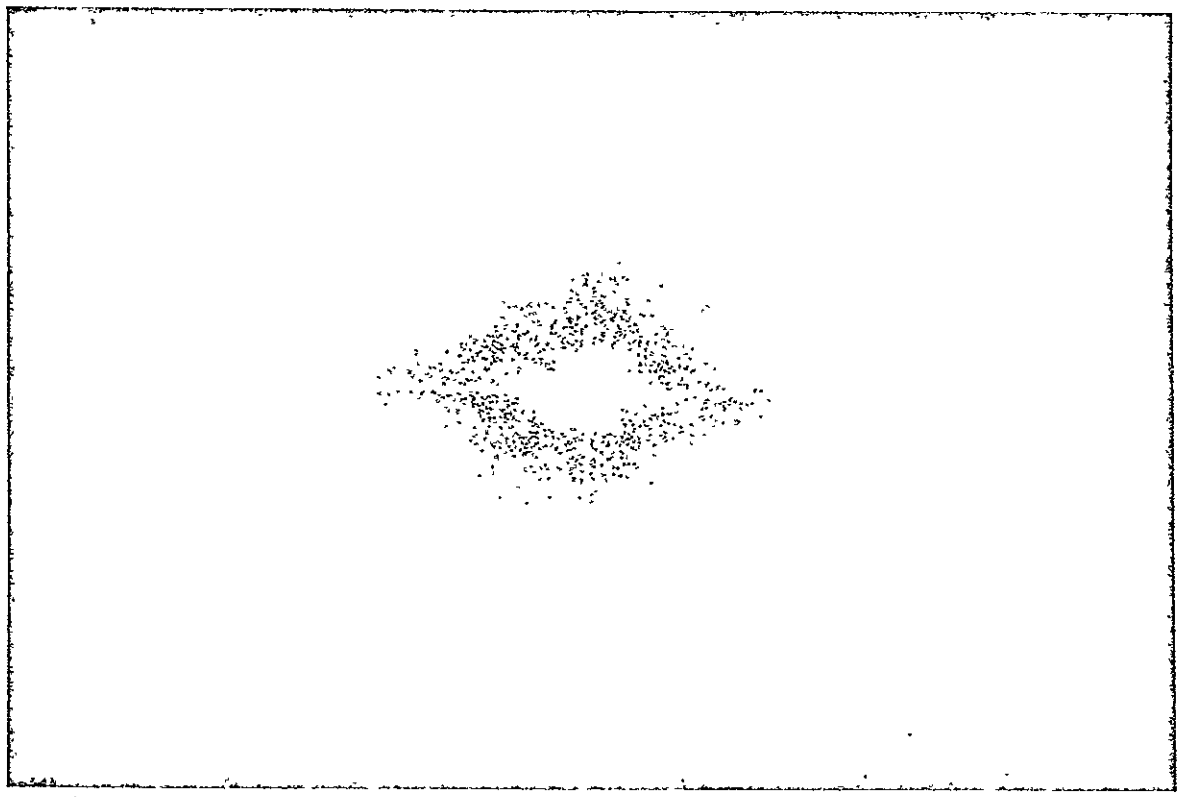

b.)

Figure 23. Orchard (0132055, #2) a) image b) power spectrum

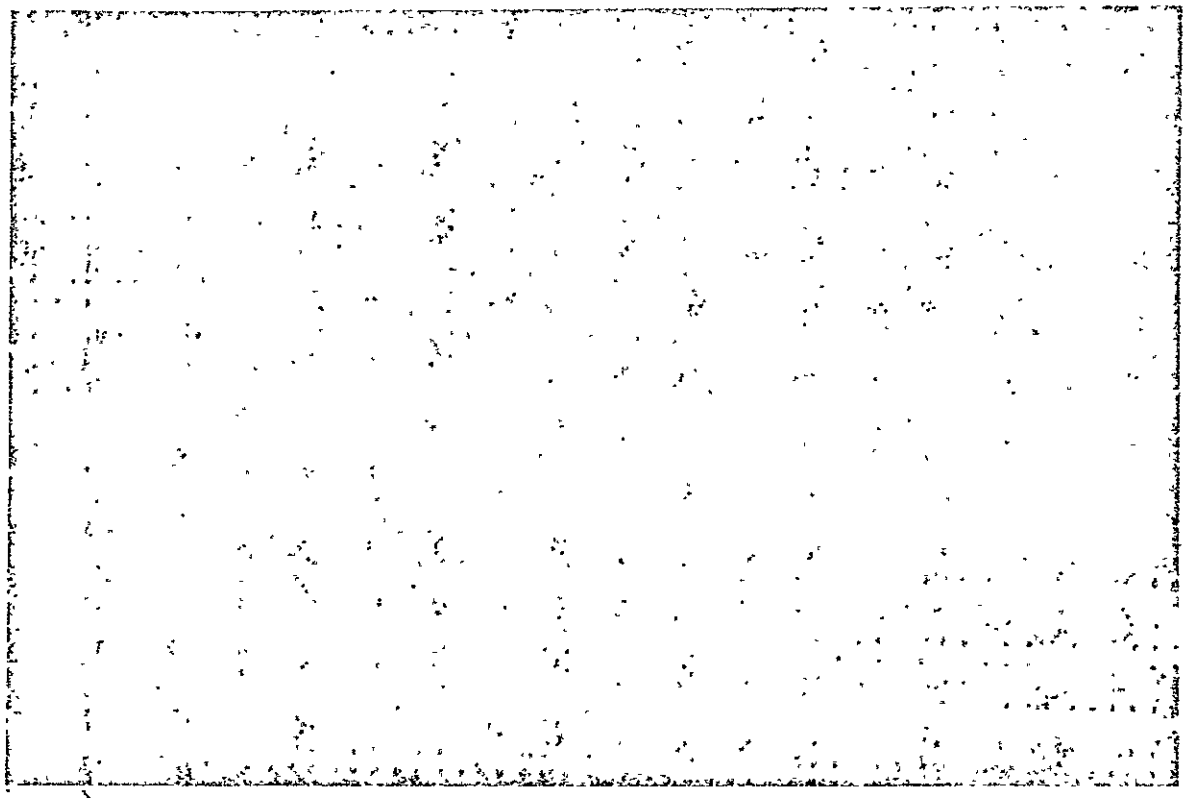

a.)

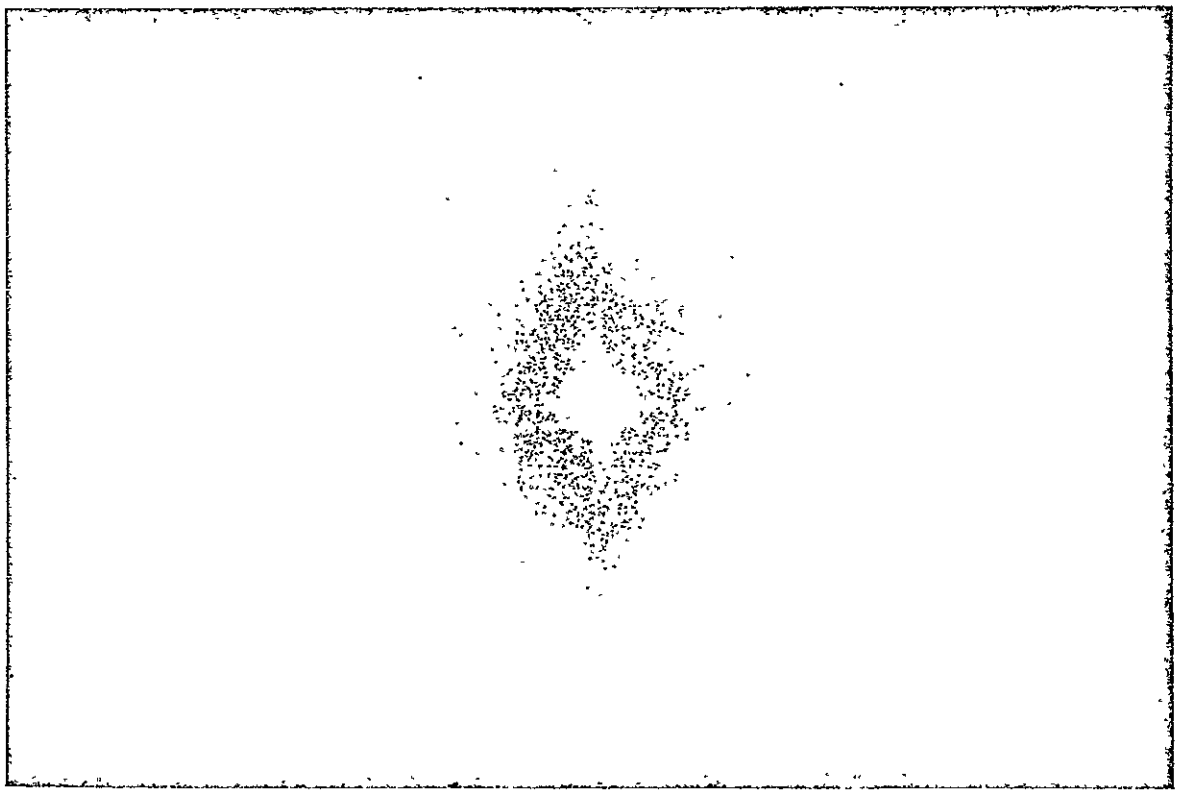

b.)

Figure 24. Peach Orchard (01320120, #2) a) image b) power spectrum

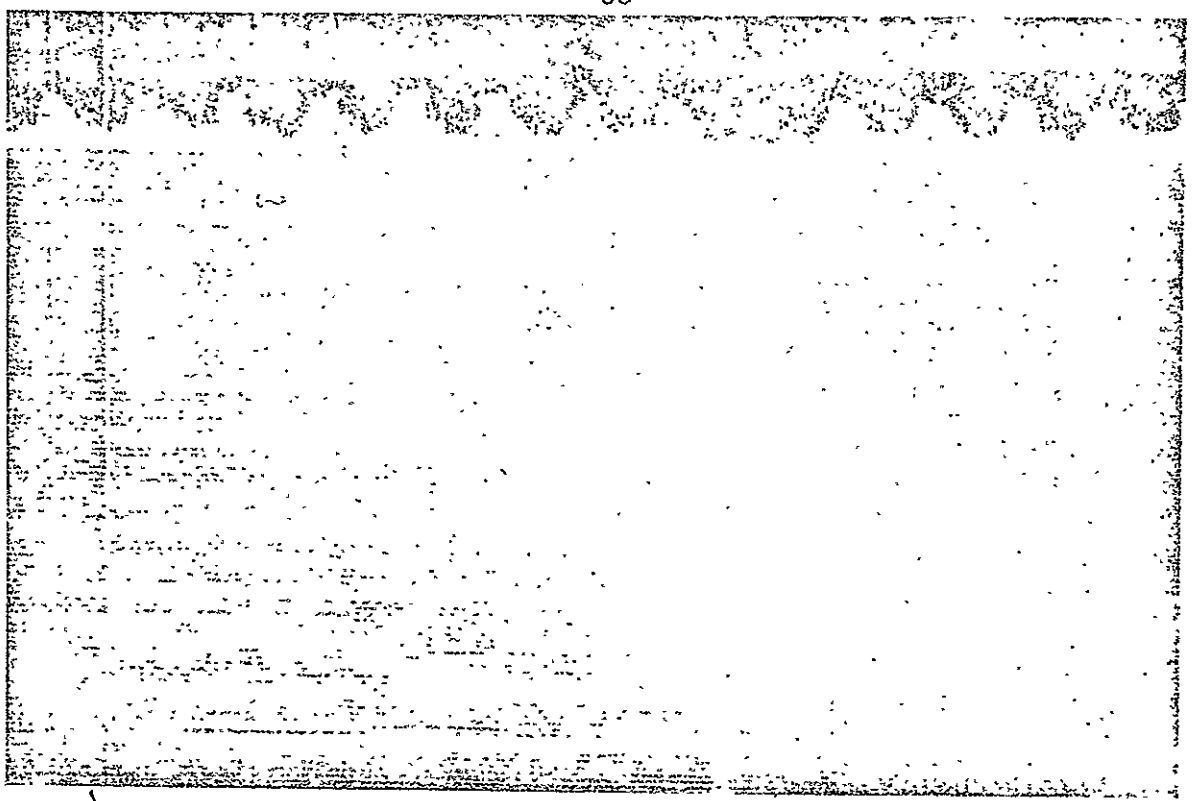

a.)

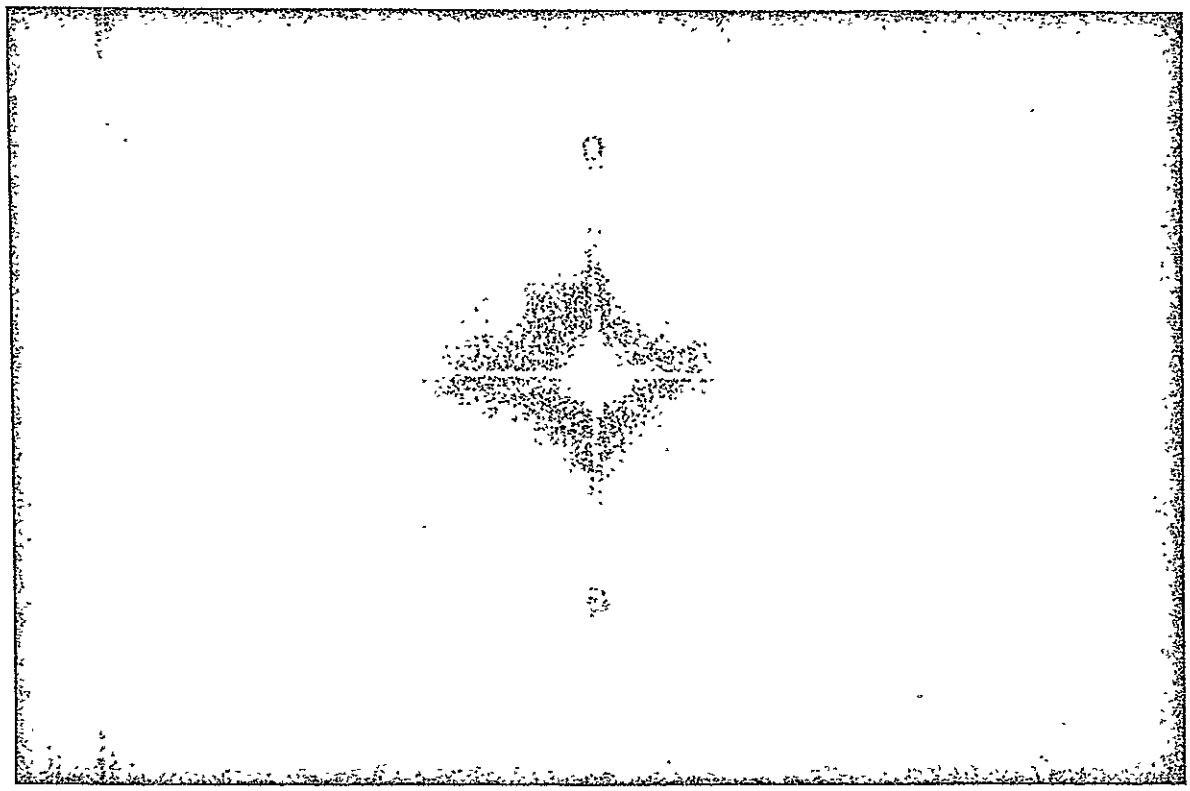

b.)

Figure 25. Plowed field (01320120, #4) a) image b) power spectrum

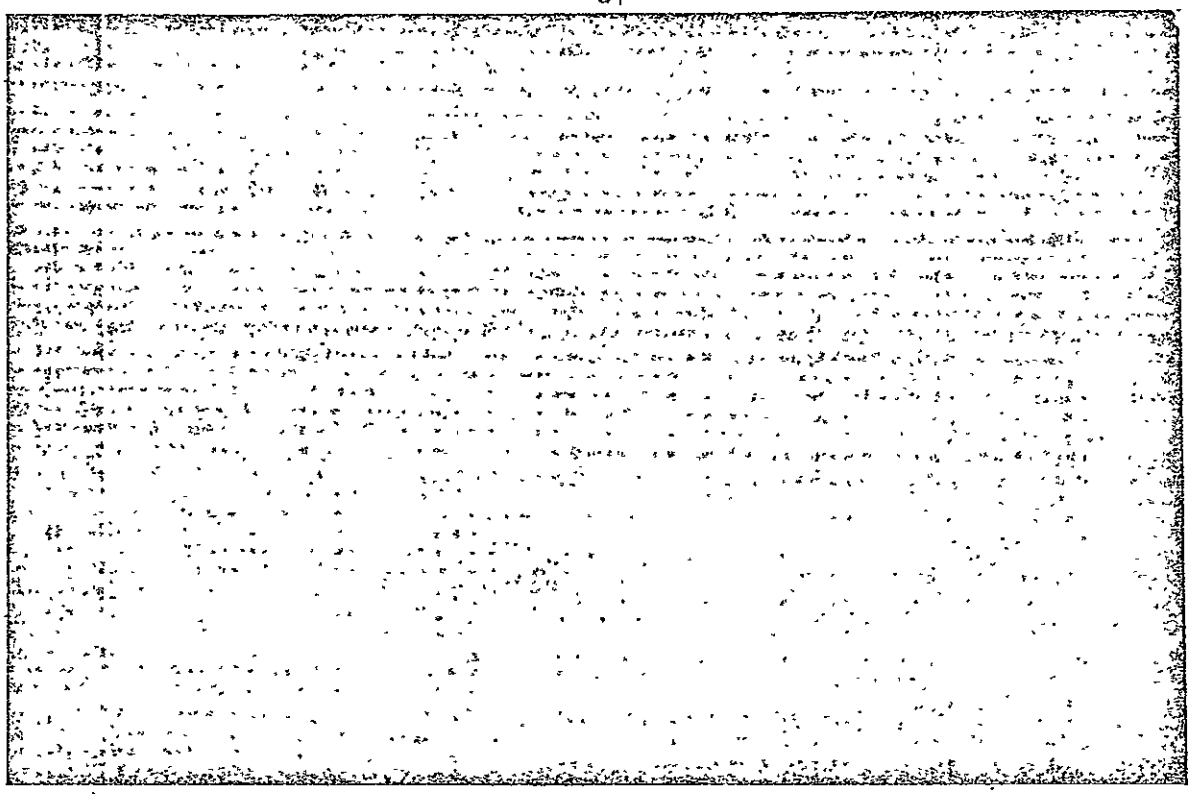

a.)

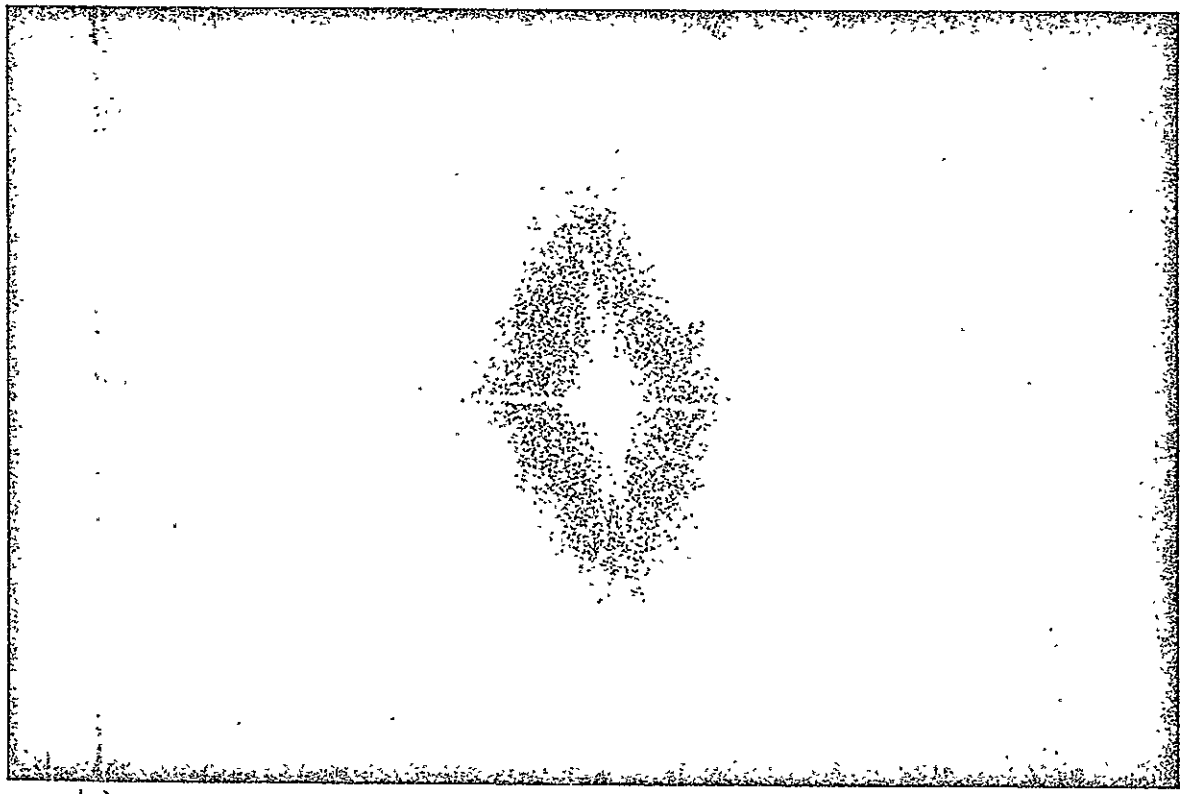

b.)

Figure 26. Sparsely populated orchard (01320120, #1) a) image b) power spectrum

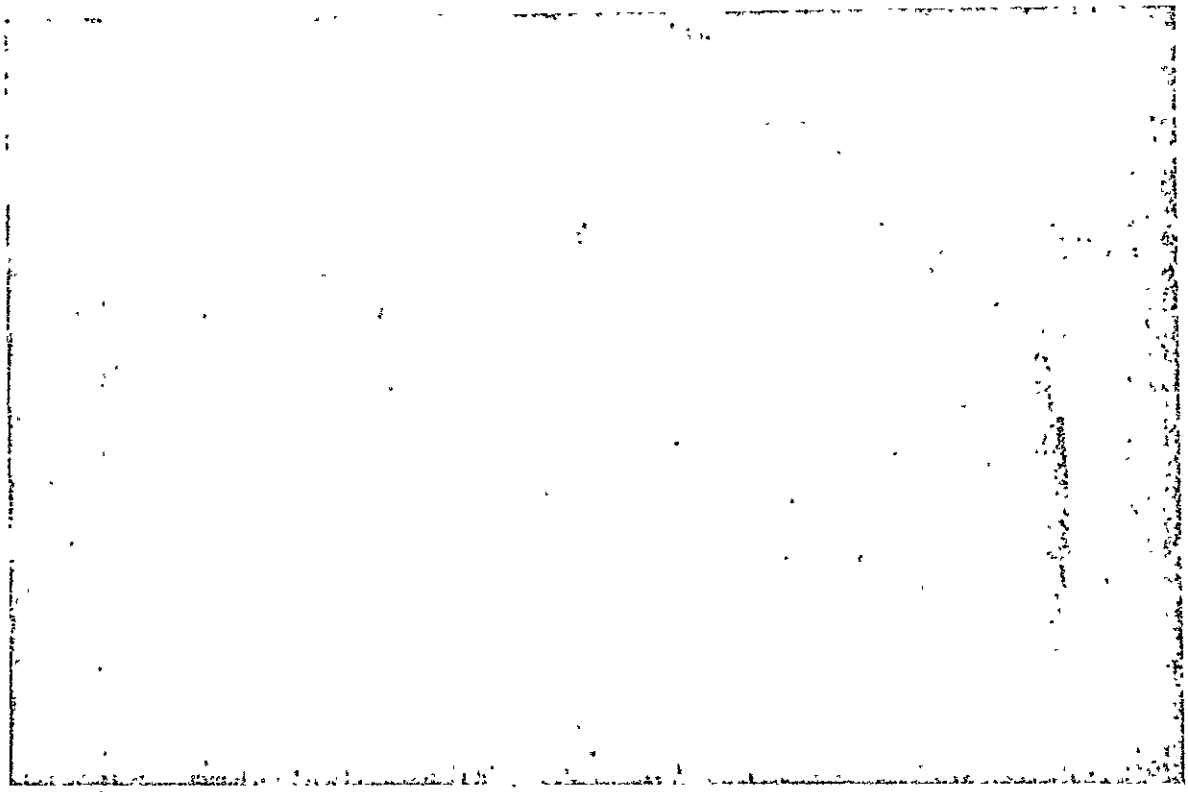

a.)

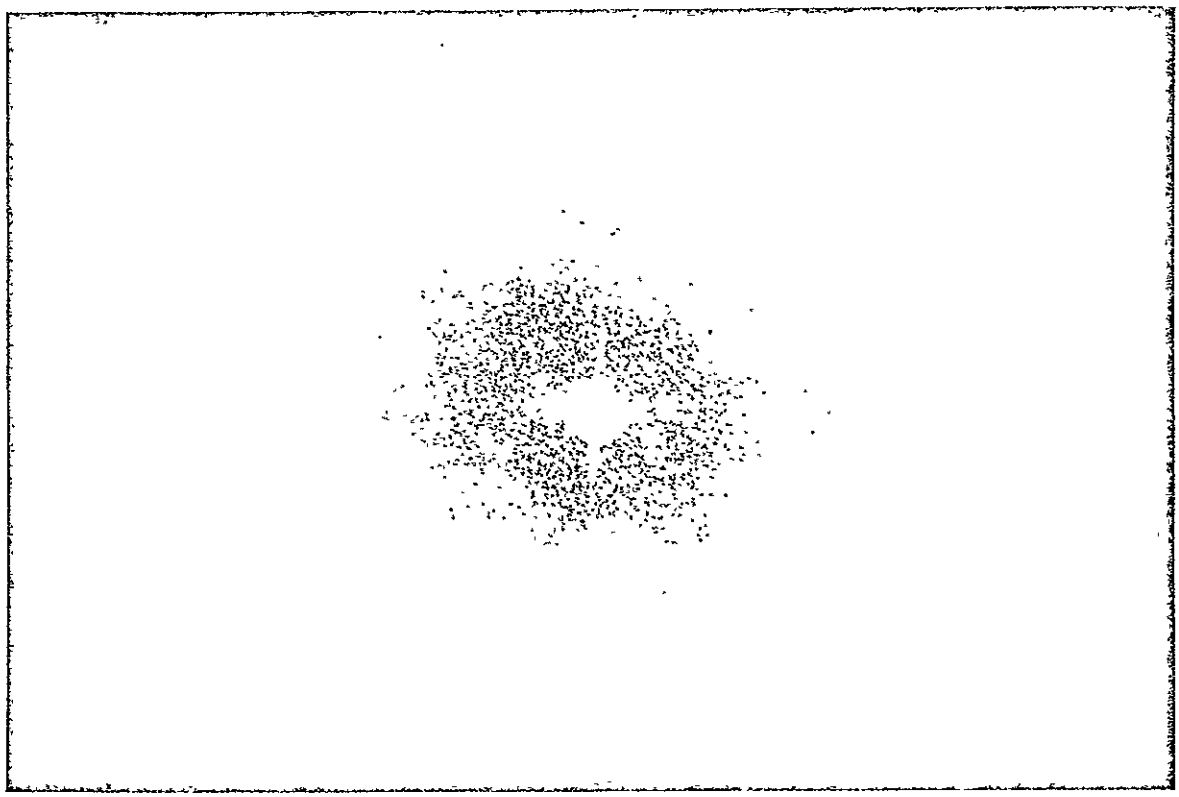

b.)

Figure 27. Composite terrain (01320120, #3) a) image b) power spectrum

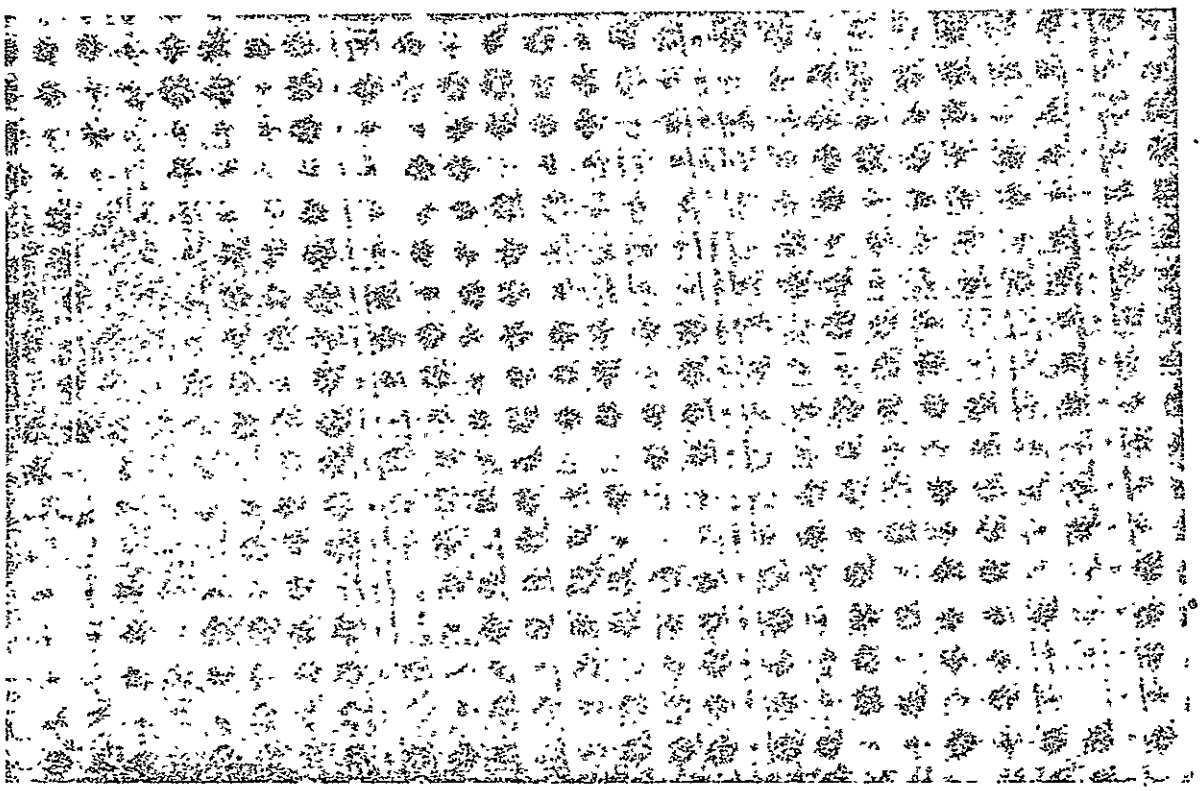

a.)

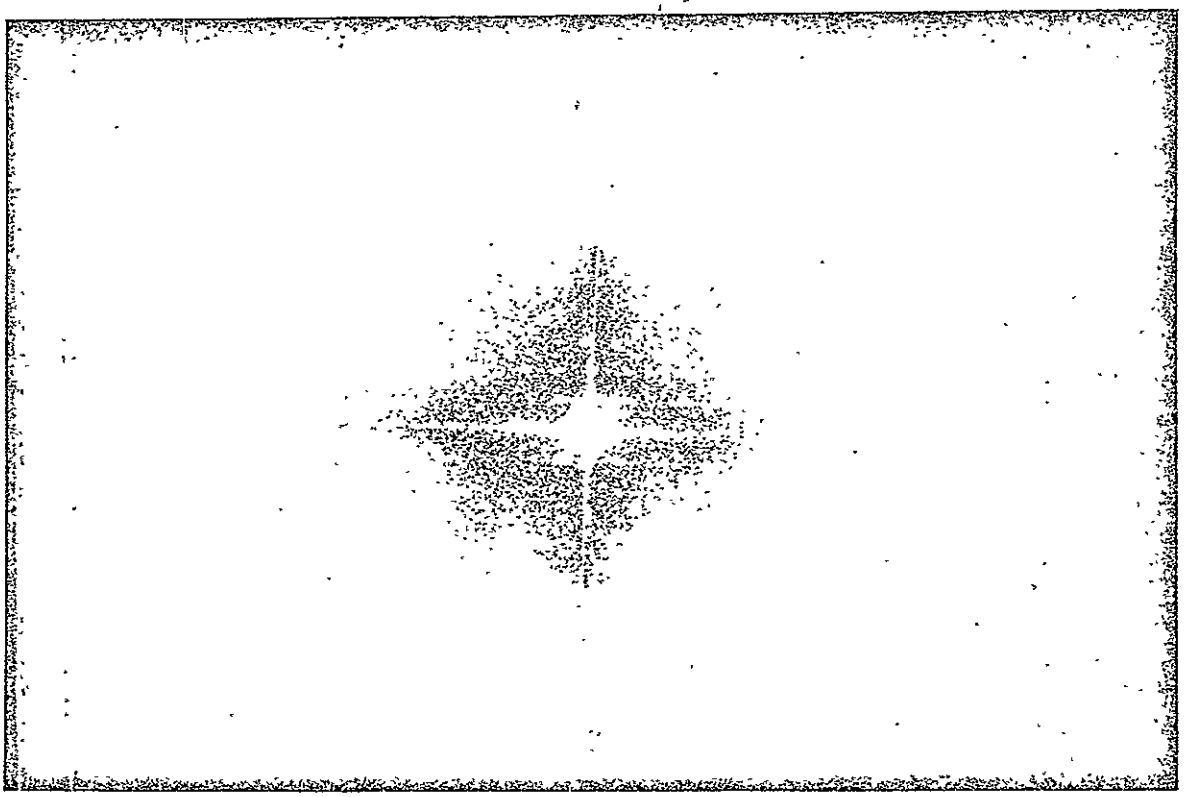

b.)

Figure 28. Peach orchard, various tree sizes (01320063, #2) a) image b) power spectrum

4.0 COMPUTER ANALYSIS

Computer programs for computing the two-dimensional Fourier transform and providing a three dimensional perspective plot were generated. The purpose was to investigate the feasibility of generating computer results for comparison with expected optical transforms. The programs were successfully operated, the major limitation being, as expected, limited resolution because of core and time requirements. However for relatively low resolution imagery the program does provide transform and correlation results. In order to use the programs effectively in analysis of images it is necessary that the imagery be scanned and digitized. Equipment for performing the scan and digitization as well as transform and filtering operations is available commercially at significant cost.

For this project, fortran programs were generated using the standard IBM FFT subroutine HARM which accepts two dimensional or even three dimensional data sets. Additionally a program suitable for operation on smaller computers which utilizes manipulation of two dimensional data in a one dimensional FFT algorithm was implemented. The procedure is to first transform the rows of a two dimensional data matrix and then transform the columns.

Arrays up to 128 x 128 were transformed and plotted on the IBM 370 and Calcomp Plotter. CPU time and core requirements for the array sizes were approximately as follows:

array size	CPU time	core
128 x 128	30-40 sec	394K
64 x 64	25-35 sec	150K

Example outputs are shown below:

Figure 29. Calculation and plot of magnitude of Fourier Transform of square aperture (64 x 64 array).

Figure 30. Calculation and plot of magnitude of Fourier Transform of circular aperture (128 x 128 array). Larger size array is used for more accuracy in image definition; however, only the central (64 x 64) portion of the transform is plotted.

Figure 31. Expanded quadrant plot of the spectrum for a circular aperture.

Figure 32. Spectrum for a narrow slit parallel to the y axis.

Figure 33. Spectrum for a narrow slit parallel to the x axis.

Figure 34 and Figure 35. Optically generated spectra for the rectangular and circular apertures.

The computer program listings are given in Appendix B.

Figure 29.

2-D FOURIER TRANSFORM

$$f(\underset{\sim}{x}) \Leftrightarrow F(\underset{\sim}{k})$$

$$F(k_x, k_y) = a_x a_y \, \mathrm{SINC}(k_x a_x) \mathrm{SINC}(k_y a_y)$$

$$F(\underset{\sim}{k}) = a_x a_y \, \mathrm{SINC}(\underset{\sim}{k}\,\underset{\sim}{a})$$

$$F(\underset{\sim}{k}) = \underset{\sim}{a} \, \mathrm{SINC}(\underset{\sim}{k}\,\underset{\sim}{a})$$

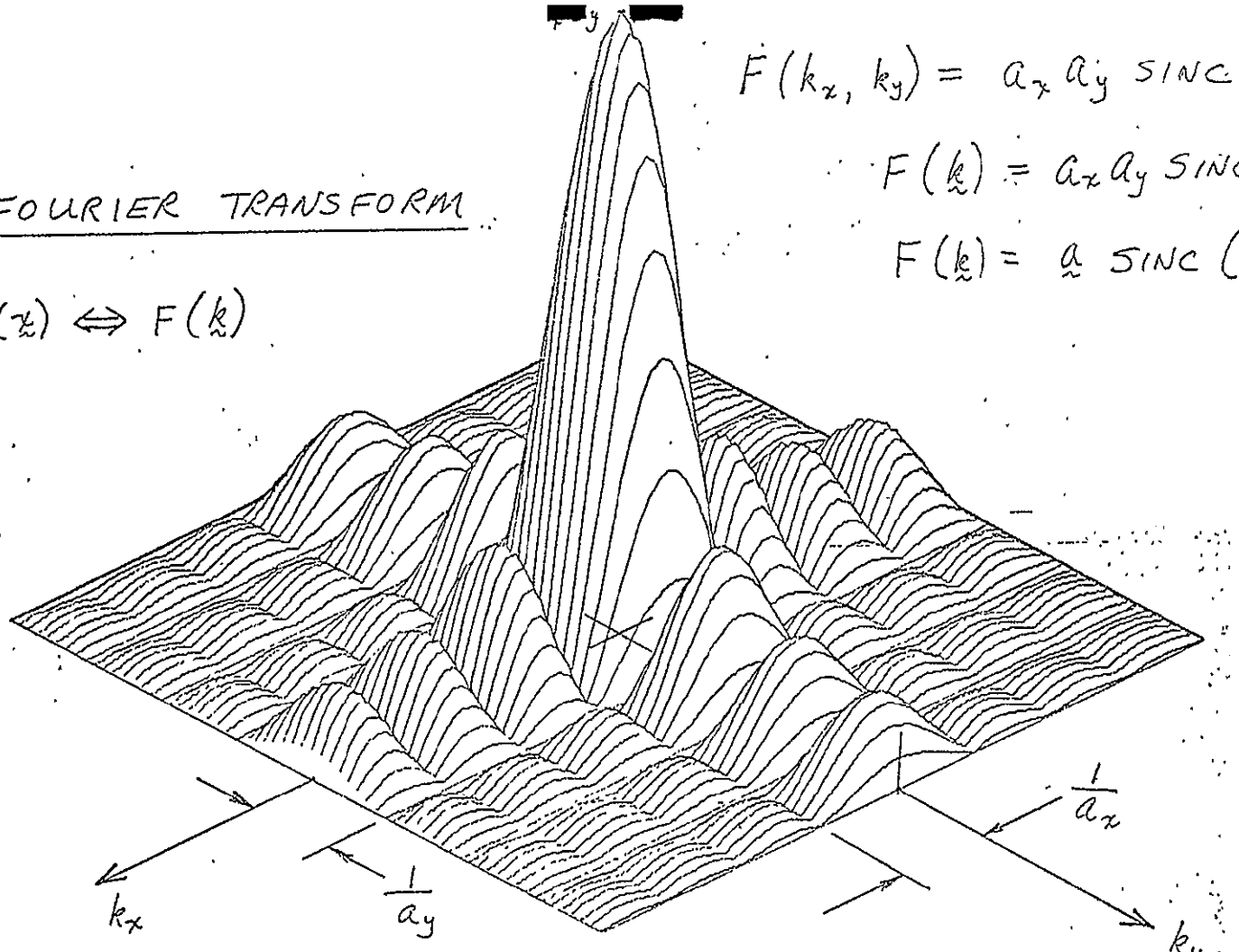

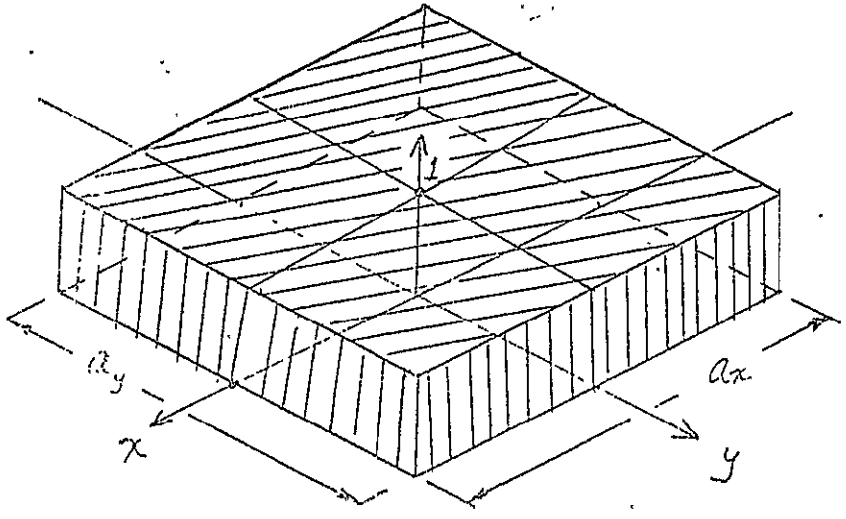

$$f(x, y) = \mathrm{RECT}\left(\frac{x}{a_x}\right) \mathrm{RECT}\left(\frac{y}{a_y}\right)$$

$$f(\underset{\sim}{x}) = \mathrm{RECT}\left(\frac{\underset{\sim}{x}}{\underset{\sim}{a}}\right)$$

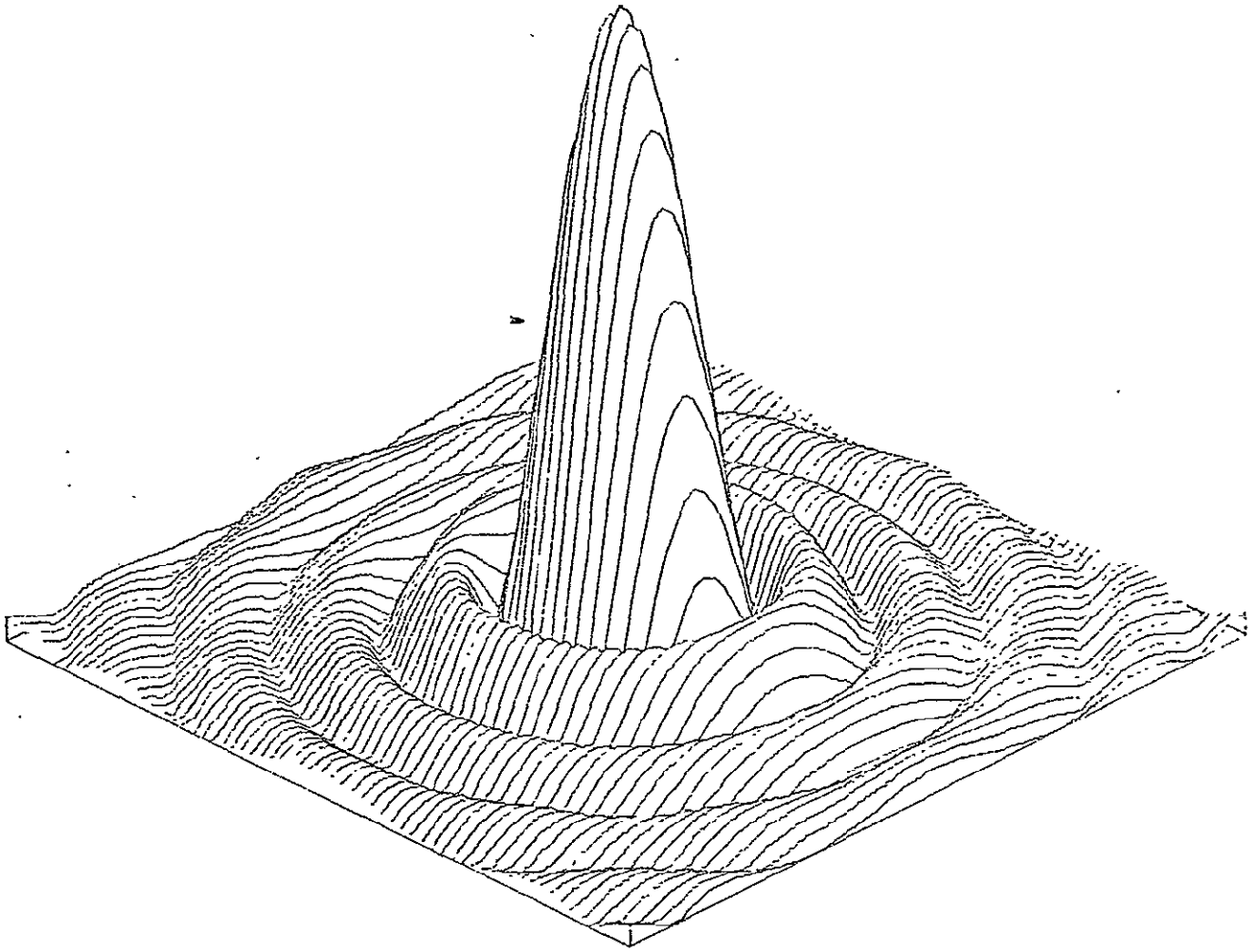

Figure 30. Magnitude plot, Fourier transform of a circular aperture.

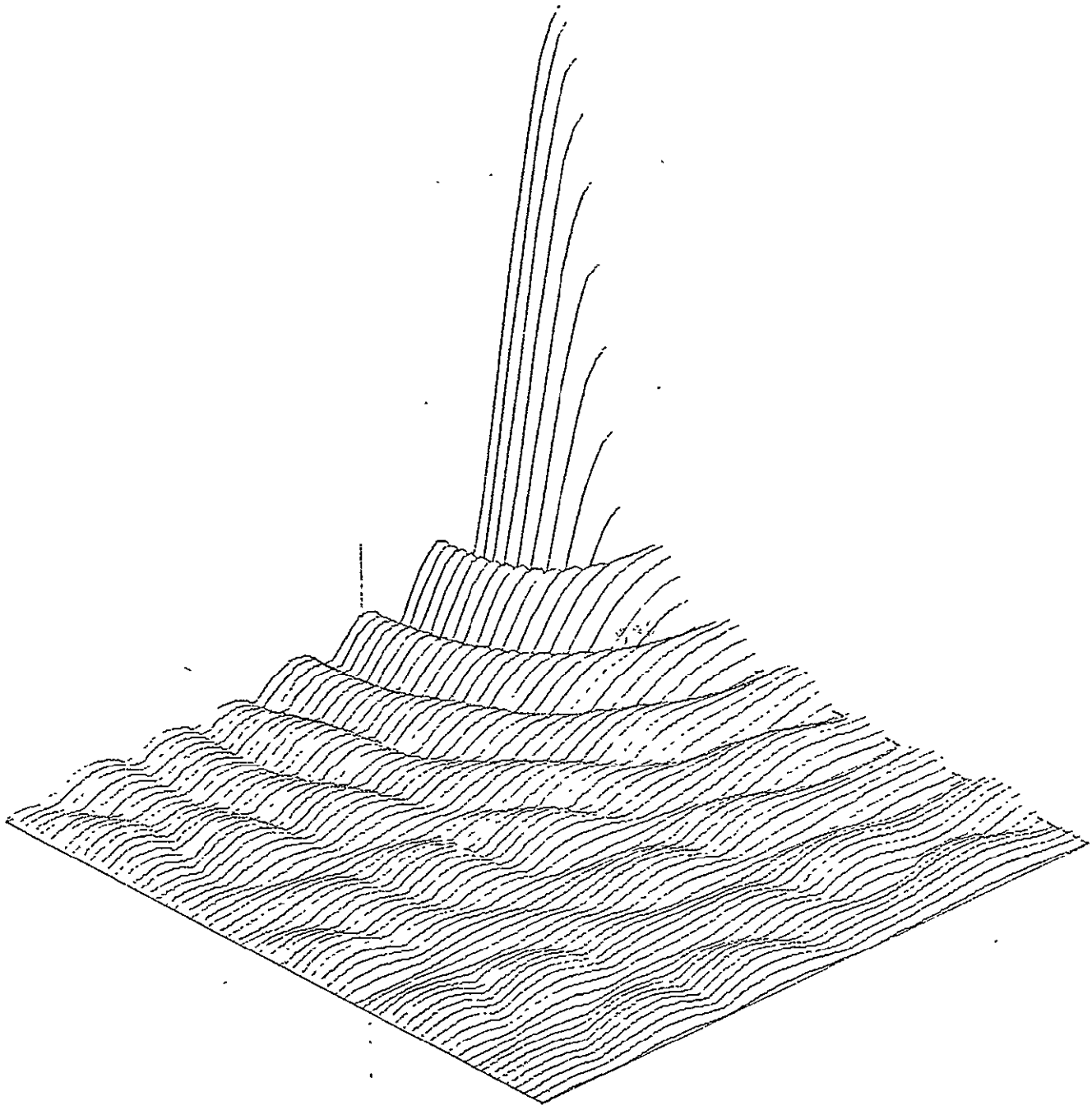

Figure 31. Expanded quadrant, magnitude spectrum for a circular aperture.

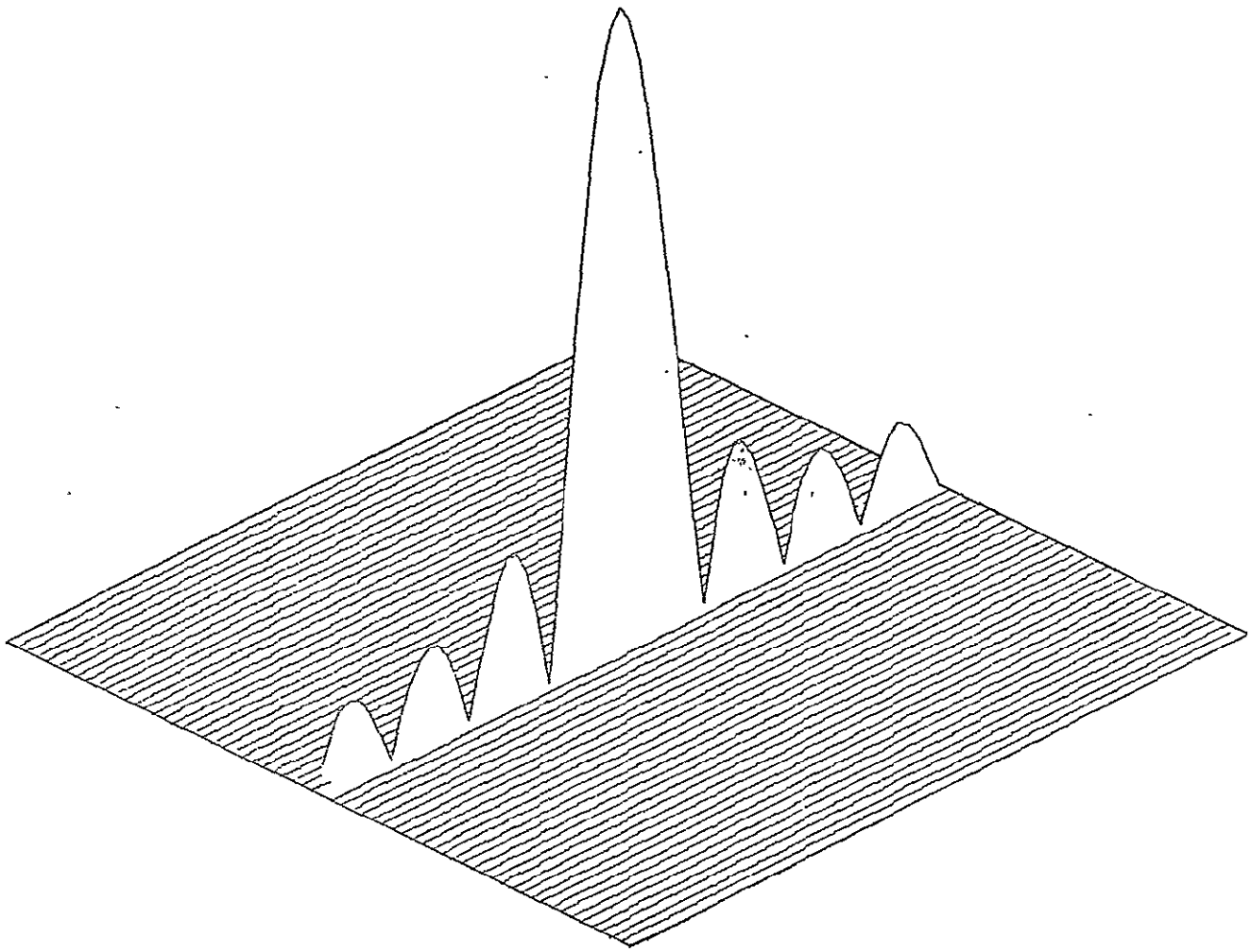

Figure 32. . Spectrum for narrow slit parallel to the x-axis.

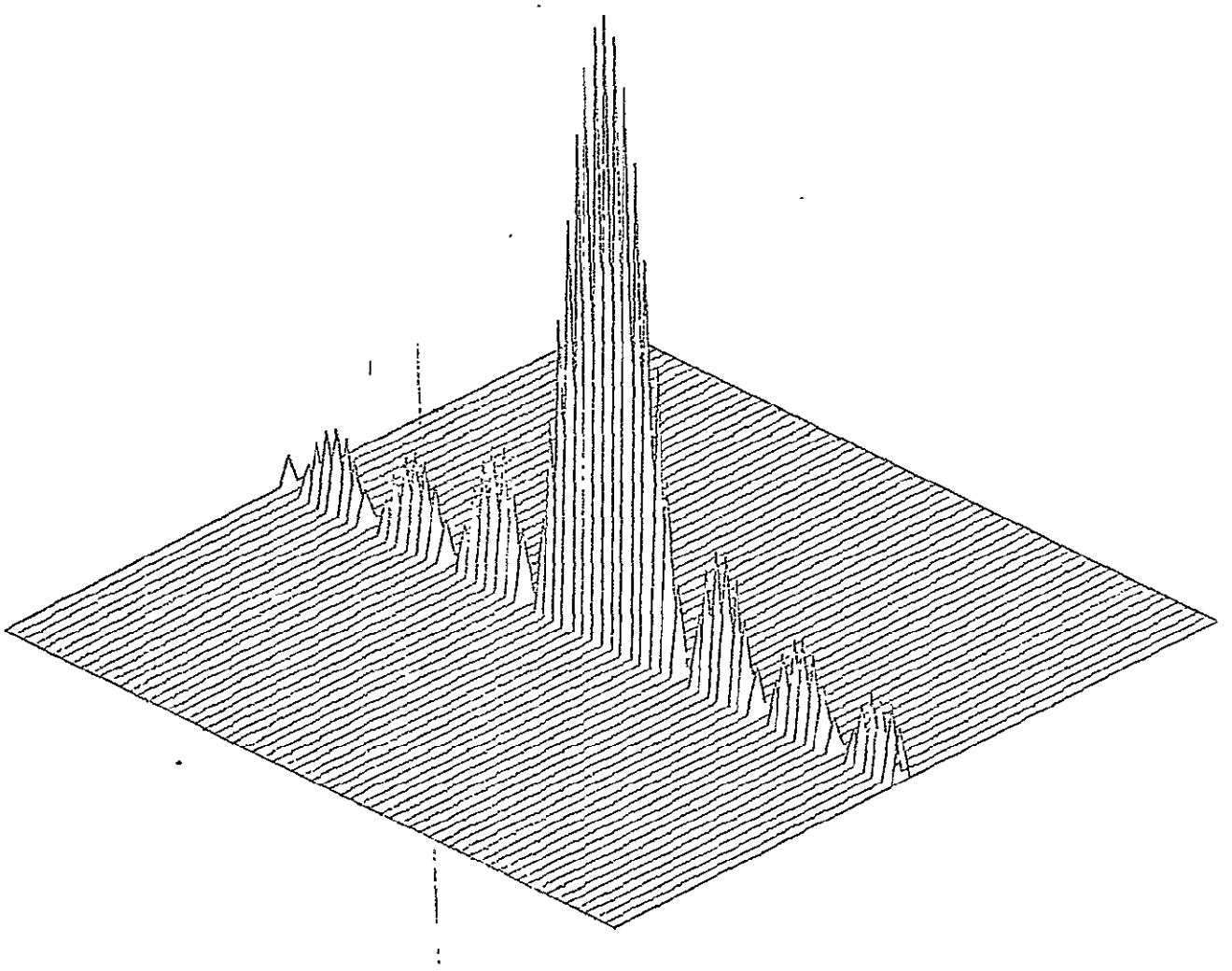

Figure 33. Spectrum for a narrow slit parallel to the y-axis.

5.0 CONCLUSIONS

The theoretical development for optical processing is based on a number of assumptions and approximations. Examination of the parametric effects of these assumptions and approximations indicates very little error in the presentation of transforms and correlations. However, other parameters, specifically errors in alignment, can be shown to have a strong effect on the success of optical processing techniques. This conclusion was predicted from parametric considerations and verified experimentally.

A major problem in the experimental implementation of optical correlators, in addition to the alignment problem, is due to the fact that the spatial frequency content of most imagery is clustered near the optical axis giving a very bright central spot. Any optical detection medium such as film then has the requirement of responding to optical patterns with a wide dynamic range. Saturation effects are almost a certainty if exposure is increased to detect the weaker pattern regions.

Further efforts at application of coherent optical processing techniques in other than a laboratory environment requires solution of practical problems.

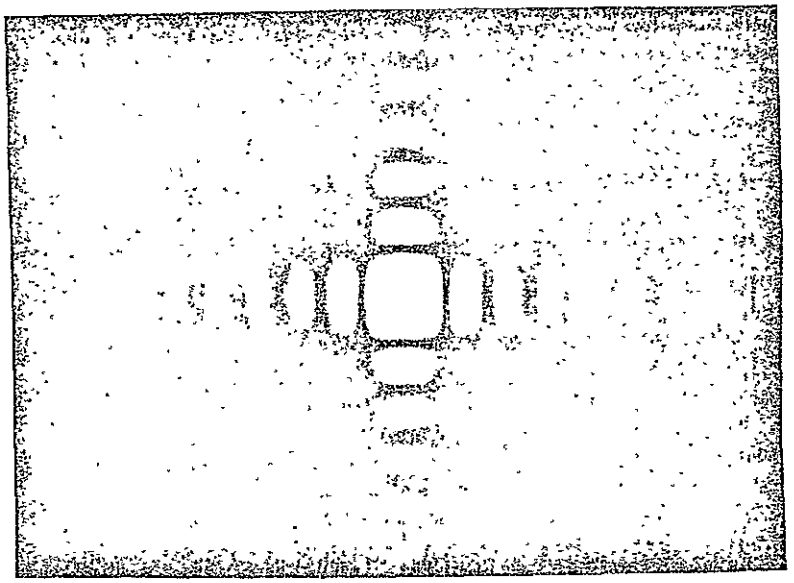

Figure 34. Optically generated spectrum for a rectangular aperture.

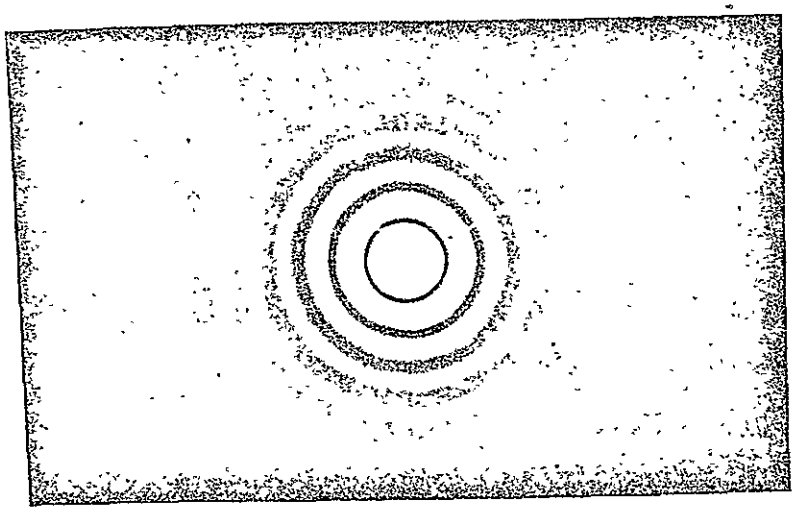

Figure 35. Optically generated spectrum for a circular aperture.

APPENDIX A: FRESNEL TRANSFORMS

A Fresnel function is defined as

$$f(\underset{\sim}{x}) \triangleq e^{i\pi a \underset{\sim}{x}^2} = e^{i\pi a(x^2+y^2)} \tag{A1}$$

where a is positive and real. Its Fourier transform is found from

$$F(\underset{\sim}{\beta}) = \int d\underset{\sim}{x}\, e^{-2\pi i \underset{\sim}{\beta}\cdot\underset{\sim}{x}}\, e^{i\pi a \underset{\sim}{x}^2} \tag{A2}$$

Equation (A2) can be evaluated using Fresnel integrals to obtain

$$F(\underset{\sim}{\beta}) = \frac{i}{a} e^{-i\pi \underset{\sim}{\beta}^2/a} = \frac{i}{a} e^{-i\pi(\beta^2+\gamma^2)/a} \tag{A3}$$

Similarly we have the Fourier transform pair

$$e^{-i\pi a \underset{\sim}{x}^2} \overset{F.T.}{\Longleftrightarrow} -\frac{i}{a} e^{i\pi \underset{\sim}{\beta}^2/a} \tag{A4}$$

From the convolution theorem and the above

$$e^{i\pi a \underset{\sim}{x}^2} * e^{-i\pi a \underset{\sim}{x}^2} = a^{-2}\,\delta(\underset{\sim}{x}) \tag{A5}$$

Now define the Fresnel transform of $g(\underset{\sim}{x})$

$$\check{g}(\underset{\sim}{x}) \triangleq g(\underset{\sim}{x}) * \left[-ia\, e^{i\pi a \underset{\sim}{x}^2}\right] \tag{A6}$$

where $\check{g}(\underset{\sim}{x})$ is the Fresnel transform of $g(\underset{\sim}{x})$. Using property (A5) it is easy to show that

$$g(\underset{\sim}{x}) = \check{g}(\underset{\sim}{x}) * \left[ia\, e^{-i\pi a \underset{\sim}{x}^2}\right] \tag{A7}$$

(A6) and (A7) define a Fresnel transform pair.

Comparison of Fourier and Fresnel transforms

If we Fourier transform both $g(\underset{\sim}{x})$ and its Fresnel transform $\check{g}(\underset{\sim}{x})$ we get

$$G(\underset{\sim}{\beta}) = \int_{-\infty}^{\infty} d\underset{\sim}{x}\; e^{-2\pi i \underset{\sim}{\beta}\cdot\underset{\sim}{x}}\; g(\underset{\sim}{x}) \tag{A8}$$

$$\check{G}(\underset{\sim}{\beta}) = \int_{-\infty}^{\infty} d\underset{\sim}{x}\; e^{-2\pi i \underset{\sim}{\beta}\cdot\underset{\sim}{x}}\; \check{g}(\underset{\sim}{x}) \tag{A9}$$

Substituting (A6) into (A9) gives

$$\check{G}(\underset{\sim}{\beta}) = \int_{-\infty}^{\infty} d\underset{\sim}{x}\; e^{-2\pi i \underset{\sim}{\beta}\cdot\underset{\sim}{x}} \left[g(\underset{\sim}{x}) * (-ia) e^{i\pi a \underset{\sim}{x}^2} \right] \tag{A10}$$

$$= \mathcal{F}\{ g(\underset{\sim}{x}) \}\; \mathcal{F}\{ -ia\, e^{i\pi a x^2} \}$$

THEN $$\check{G}(\underset{\sim}{\beta}) = G(\underset{\sim}{\beta})(-ia)\left(\frac{i}{a}\right) e^{-i\pi \underset{\sim}{\beta}^2/a}$$

or $$\check{G}(\underset{\sim}{\beta}) = G(\underset{\sim}{\beta})\, e^{-i\pi \underset{\sim}{\beta}^2/a} \tag{A11}$$

Equation (A11) says that a Fresnel transform in the spatial domain corresponds to a multiplicative phase factor in the spatial frequency domain.

Fresnel transforms are useful in describing propagating optical fields and in the study of Fresnel diffraction.

APPENDIX B:

COMPUTER LISTINGS

```
C      PROGRAM USING SUBROUTINES FFT AND PLOT3D
       COMPLEX A(64),U,W,T,F(64,64),C(64,64)
       DIMENSION OUTBUF(64),MASK(2000),VERTEX(16)
       N=64
       M=6
C      C(I,J) IS INITIALLY THE COMPLEX N X N ARRAY TO BE
C      FOURIER TRANSFORMED
C      A(I) IS THE ONE DIMENSIONAL N-ELEMENT ARRAY ON WHICH
C      SUBROUTINE FFT OPERATES
C      U,W,AND T ARE VARIABLES OF SUBROUTINE FFT
C      OUTBUF,MASK,AND VERTEX ARE ARRAYS OF SUBROUTINE PLOT3D
C      FORM INPUT ARRAY FOR SQUARE APERTURE
       DO 1 I=1,N
       DO 1 J=1,N
       C(I,J)=0.0
       IF (J.GE.29.AND.J.LE.36.AND.I.GE.29.AND.I.LE.36)
      *C(I,J)=1.0
     1 CONTINUE
C      PERFORM ONE DIMENSIONAL FFT ON ROWS OF C(I,J) AND
C      STORE RESULT IN F(I,J)
       DO 4 I=1,N
       DO 2 J=1,N
     2 A(J)=C(I,J)
       CALL FFT(A,M,N)
       DO 3 K=1,N
       K1=N-K+1
     3 F(I,K1)=A(K)
     4 CONTINUE
C      EACH OF THE N-ELEMENT ONE DIMENSIONAL TRANSFORMS NOW
C      FORMS A ROW OF F(I,J)
C      TAKE TRANSFORM OF COLUMNS OF F(I,J) AND STORE RESULT
C      IN C(I,J)
       DO 5 J=1,N
       DO 6 I=1,N
     6 A(I)=F(I,J)
       CALL FFT(A,M,N)
       DO 7 K=1,N
       K1=N-K+1
     7 C(K1,J)=A(K)
     5 CONTINUE
C      TRANSFORM IS NOW STORED IN C(I,J). TAKE ABSOLUTE VALUE
C      OF EACH COMPLEX ENTRY
       DO 8 I=1,N
       DO 8 J=1,N
     8 C(I,J)= CABS(C(I,J))
C      REARRANGE FOR PROPER OUTPUT AND STORE IN ARRAY F(I,J)
       ND2=N/2
       ND2M1=ND2-1
       ND2P1=ND2+1
       ND2P2=ND2+2
```

```
      DO 71 I=1,ND2P1
      DO 71 J=1,ND2P1
   71 F(I+ND2M1,J+ND2M1)=C(I,J)
      DO 72 I=ND2P2,N
      DO 72 J=1,ND2P1
   72 F(I-ND2P1,J+ND2M1)=C(I,J)
      DO 73 I=ND2P2,N
      DO 73 J=ND2P2,N
   73 F(I-ND2P1,J-ND2P1)=C(I,J)
      DO 74 I=1,ND2P1
      DO 74 J=ND2P2,N
   74 F(I+ND2M1,J-ND2P1)=C(I,J)
C     NORMALIZE VALUES IN F(I,J) TO VALUE OF ONE
      FMAX=0.0
      DO 21 I=1,N
      DO 21 J=1,N
      IF (FMAX.GE.CABS(F(I,J))) GO TO 21
      FMAX=F(I,J)
   21 CONTINUE
      DO 22 I=1,N
      DO 22 J=1,N
      F(I,J)=F(I,J)/FMAX
   22 CONTINUE
C     PLOT THE ARRAY F(I,J) USING SUBROUTINE PLOT3D
      DO 20 NLINE=1,N
      DO 10 NPOINT=1,N
      OUTBUF(NPOINT)=F(NPOINT,NLINE)
   10 CONTINUE
      CALL PLOT3D(1010,0.0,OUTBUF,0.0,0.075,4.0,-0.075,
     *NLINE,64,-45.0,-30.0,5.0,3.0,10.0,MASK,VERTEX)
   20 CONTINUE
C     DRAW FRAME AROUND PLOT USING SUBROUTINE FRAMER
      CALL FRAMER(3,VERTEX,MASK)
C     SIGNAL THAT PLOT IS COMPLETE
      CALL PLOT(0.0,0.0,999)
      STOP
      END
```

```
      SUBROUTINE FFT(A,M,N)
      COMPLEX A(:),U,W,T
      N= 2**M
      NV2=N/2
      NM1=N-1
      J=1
      DO 7 I=1,NM1
      IF(I.GE.J) GO TO 5
      T=A(J)
      A(J)=A(I)
      A(I) =T
    5 K=NV2
    6 IF(K.GE.J) GO TO 7
      J=J-K
      K=K/2
      GO TO 6
    7 J=J+K
      PI=3.14159
      DO 20 L=1,M
      LE=2**L
      LE1=LE/2
      U=(1.0,0.)
      W=CMPLX(COS(PI/LE1),SIN(PI/LE1))
      DO 20 J=1,LE1
      DO 10 I=J,N,LE
      IP=I+LE1
      T=A(IP)*U
      A(IP)=A(I)-T
   10 A(I)=A(I)+T
   20 U=U*W
      RETURN
      END
```

```
C     PROGRAM USING SUBROUTINES HARM AND PLOT3D
      DIMENSION A(32768),M(3),INV(4096),Y(128,128),
     *X(128,128),S(4096),IVAL(128),MASK(2000),VERTEX(16),
     *OUTBUF(128)
      N=128
      NSQD=N**2
      NSQDT2= 2*NSQD
C     FORM INPUT ARRAY X(I,J) TO BE FOURIER TRANSFORMED
C     AND COLUMNIZE TO ARRAY A(I) FOR INPUT TO SUBROUTINE
C     HARM
      K=1
      DO 1 J=1,N
      DO 1 I=1,N
C     FORM INPUT ARRAY FOR CIRCULAR APERTURE
      X(I,J)=0.0
      IF (J.GE.62.AND.J.LE.67.AND.I.GE.57
     *.AND.I.LE.72) X(I,J)=1.0
      IF ((J.EQ.57.OR.J.EQ.72) .AND.I.GE.62.AND.
     *I.LE.67) X(I,J)=1.0
      IF ((J.EQ.58.OR.J.EQ.71) .AND.I.GE.60.AND.
     *I.LE.69) X(I,J)=1.0
      IF ((J.EQ.59.OR.J.EQ.70) .AND.I.GE.59.AND.
     *I.LE.70) X(I,J)=1.0
      IF ((J.EQ.60.OR.J.EQ.61.OR.J.EQ.68.OR.
     *J.EQ.69) .AND.I.GE.58.AND.I.LE.71) X(I,J)=1.0
      A(K)= X(I,J)
      A(K+1)=0.0
      K=K+2
    1 CONTINUE
C     SET UP PARAMETERS FOR SUBROUTINE HARM
      IFSET=1
      M(1)=7
      M(2)=7
      M(3)=0
      CALL HARM(A,M,INV,S,IFSET,IFERR)
C     CHECK FOR ERRORS
      IF (IFERR.NE.0) GO TO 35
      GO TO 60
   35 WRITE(6,50) IFERR
   50 FORMAT ('1',30(/),56X,'IFERR=',I2)
      STOP
C     PUT THE COMPLEX TRANSFORMED ARRAY A(I) INTO NEW
C     MAGNITUDE ARRAY A(I)
   60 DO 65 I=1,NSQDT2,2
   65 A((I+1)/2)= SQRT((A(I))**2+(A(I+1))**2)
C     PUT ARRAY A(I) INTO TWO DIMENSIONAL ARRAY Y(I,J)
      I=0
      DO 70 L=1,N
      DO 70 J=1,N
      I=I+1
   70 Y(J,L)= A(I)
C     REARRANGE FOR PROPER OUTPUT AND STORE IN ARRAY X(I,J)
      ND2=N/2
      ND2M1=ND2-1
      ND2P1=ND2+1
      ND2P2=ND2+2
      DO 71 I=1,ND2P1
      DO 71 J=1,ND2P1
```

```
   71 X(I+ND2M1,J+ND2M1)=Y(I,J)
      DO 72 I=ND2P2,N
      DO 72 J=1,ND2P1
   72 X(I-ND2P1,J+ND2M1)=Y(I,J)
      DO 73 I=ND2P2,N
      DO 73 J=ND2P2,N
   73 X(I-ND2P1,J-ND2P1)=Y(I,J)
      DO 74 I=1,ND2P1
      DO 74 J=ND2P2,N
   74 X(I+ND2M1,J-ND2P1)=Y(I,J)
C     NORNALIZE VALUES IN X(I,J) TO VALUE OF ONE
      XMAX=0.0
      DO 21 I=1,N
      DO 21 J=1,N
      IF (XMAX.GE.X(I,J)) GO TO 21
      XMAX=X(I,J)
   21 CONTINUE
      DO 22 I=1,N
      DO 22 J=1,N
      X(I,J)=X(I,J)/XMAX
   22 CONTINUE
C     PLOT THE CENTRAL 64 X 64 ELEMENTS OF THE 128 X 128
C     ARRAY X(I,J) USING SUBROUTINE PLOT3D
      DO 20 I=33,96
      DO 10 J=33,96
      NLINE=I-32
      NPOINT=J-32
      OUTBUF(NPOINT)=X(J,I)
   10 CONTINUE
      CALL PLOT3D(1010,0.0,OUTBUF,0.0,0.075,4.0,-0.075,
     *NLINE,64,-45.0,-30.0,5.0,3.0,10.0,MASK,VERTEX)
   20 CONTINUE
      CALL FRAMER(3,VERTEX,MASK)
      CALL PLOT(0.0,0.0,999)
      STOP
      END
```

ENGINEERING EXPERIMENT STATION

AUBURN UNIVERSITY

AUBURN, ALABAMA